Research Square

Preprints are preliminary reports that have not undergone peer review.
They should not be considered conclusive, used to inform clinical practice,
or referenced by the media as validated information.

Manufacturing Process Effects on Multiaxial Mechanical Behavior and Anisotropy Evolution of Fiber-Reinforced Polymer Composites for Automotive Applications

Kathir Vadivel Marimuthu
Birla Institute of Technology and Science
Riya Sharma
Birla Institute of Technology and Science
Shamsher Bahadur Singh
sbsingh@pilani.bits-pilani.ac.in

Birla Institute of Technology and Science
Rajesh Kumar
Birla Institute of Technology and Science
Sharad Shrivastava
Birla Institute of Technology and Science
Sudhirkumar V. Barai
Birla Institute of Technology and Science

Research Article

Keywords: Fiber-reinforced composites, Manufacturing process, Multiaxial mechanical characterization, Mechanical anisotropy, Automotive composites

Posted Date: July 1st, 2026

DOI: https://doi.org/10.21203/rs.3.rs-10068510/v1

License: This work is licensed under a Creative Commons Attribution 4.0 International License.
Read Full License

Additional Declarations: No competing interests reported.

Version of Record: A version of this preprint was published at Discover Materials on October 1st, 2026. See the published version at https://doi.org/10.1007/s43939-026-00987-8.

Manufacturing Process Effects on Multiaxial Mechanical Behavior and Anisotropy Evolution of Fiber-Reinforced Polymer Composites for Automotive Applications

Kathir Vadivel Marimuthu[a†], Riya Sharma[b†], Shamsher Bahadur Singh[a*], Rajesh Kumar[a], Sharad Shrivastava[b], Sudhirkumar V. Barai[a]

[a]Department of Civil Engineering, Birla Institute of Technology and Science, Pilani, Pilani campus, Rajasthan 333031, India

[b]Department of Mechanical Engineering, Birla Institute of Technology and Science, Pilani, Pilani campus, Rajasthan 333031, India

[*]Corresponding Author

[†]Both authors have equally contributed to the completion of the research article

Email id: kathir.vadivel@pilani.bits-pilani.ac.in, p20220437@pilani.bits-pilani.ac.in, sbsingh@pilani.bits-pilani.ac.in (corresponding author), rajesh.kr@pilani.bits-pilani.ac.in, sharad_shrivastava@pilani.bits-pilani.ac.in, skbarai@pilani.bits-pilani.ac.in.

Abstract: Processing-induced variations play a crucial role in defining the mechanical anisotropy and structural efficiency of fiber-reinforced polymer (FRP) composites. This study investigates the multiaxial mechanical behavior and anisotropy of unidirectional carbon (CFRP), glass (GFRP), and basalt (BFRP) epoxy composites fabricated using two controlled processing techniques: hand layup (HLU) and vacuum-assisted resin transfer molding (VARTM). Process-based density, fiber volume fraction, and void content are quantitatively correlated with tensile, compression, in-plane shear, flexural, and interlaminar shear properties. Across all fiber types, VARTM produces higher fiber volume fraction and lower void content, enhancing stiffness-dominated behaviors and interlaminar load transfer, while HLU shows improvements in longitudinal compression strength for selected laminate systems. The stiffness- and strength-based anisotropy indices indicate that the processing technique governs the directional contrast in the longitudinal, transverse, bending, and shear responses. VARTM increases tensile and compressive anisotropies in CFRP and BFRP, demonstrating fiber-dominant load transfer, while reducing compression and flexural anisotropies in GFRP due to its transverse fiber-knitting architecture. Interlaminar shear indices indicate that VARTM improves shear-transfer efficiency in CFRP and BFRP. Analysis of variance (ANOVA) confirms significant statistical effects of fiber type, manufacturing process, and their

interaction. These findings establish a clear process-structure-anisotropy relationship for understanding the effect of manufacturing process on the directional mechanical behavior of FRP laminates, guiding the design and optimization of lightweight automotive composite structures.

Highlights:

- VARTM improves microstructural quality: higher V_f and lower void content (< 2%)
- VARTM increases tensile and compression anisotropy in CFRP and BFRP
- VARTM–GFRP exhibits low compression & flexural anisotropy due to fiber architecture
- ILSS translation index decreases for VARTM–CFRP and BFRP: better delamination resistance
- ANOVA shows manufacturing affects all properties, except long. compression strength

Keywords: Fiber-reinforced composites, Manufacturing process, Multiaxial mechanical characterization, Mechanical anisotropy, Automotive composites.

1. Introduction

In modern automotive design, a lightweight design approach is a key strategy for improving fuel economy, extending electric vehicle driving range, and reducing emissions [1]. Fiber-reinforced polymer (FRP) composites have emerged as alternatives to conventional materials in many automotive components, such as door panels [2], bumper beams [3], and floor and rocker panels [4], owing to their high strength-to-weight ratio, fatigue durability, and corrosion resistance [5]. However, unlike metals, FRPs exhibit strong directional dependence (anisotropy) that is highly sensitive to the manufacturing methods. Variations in manufacturing processes result in differences in fiber compaction, fiber volume fraction, resin infiltration, and void content, which significantly influence the mechanical behavior of the composites [6]. Their suitability for automotive structures depends not only on longitudinal tensile properties but also on transverse, compressive, shear, flexural, and interlaminar responses, as these properties govern composite behavior under complex loading conditions. This is particularly important because automotive components are subjected to multiaxial loading during bending, vibration, crash, compression, torsion, and impact events [4]. Thus, for a reliable design of automotive components, it is essential to understand the process-induced mechanical behavior and the evolution of anisotropy in unidirectional FRP composites.

Traditional composite laminate manufacturing processes include hand layup (HLU), spray-up, injection molding, compression molding, resin transfer molding (RTM), and autoclave curing [7]. Among these, HLU and vacuum-assisted resin transfer molding (VARTM), a closed-mold RTM variant, represent two contrasting processing routes that inherently generate different compositional states, and thus different anisotropic mechanical responses. The HLU process, although labor-intensive, remains widely used for prototyping marine structures, laboratory-scale research, and small-scale applications due to its simplicity and low cost [8]. In contrast, VARTM offers superior control over fiber compaction and matrix infiltration, resulting in stronger fiber-resin interfacial bonding and reduced porosity [9].

Comparative studies consistently demonstrate the effect of manufacturing process on the absolute mechanical properties of FRP composites. VARTM-processed CFRP often achieved higher tensile, compressive, and flexural properties than HLU, primarily due to improved fiber-resin bonding and reduced void content [10-12]. Although the improvements in longitudinal properties are noted, the studies did not measure or analyze corresponding transverse properties to quantify anisotropy. Similarly, GFRP also demonstrated improvements in longitudinal tensile, compression, flexural, and interlaminar shear properties with VARTM, emphasizing the roles of reduced void content, higher fiber volume, and improved fiber wetting [13-16]. Similarly, BFRP, despite its high tensile strength, good thermal resistance, cost-effectiveness, and eco-friendly production method, remains comparatively unexplored [17]. Several studies reported improvements in the tensile, flexural, and interlaminar shear properties of BFRP under VARTM [18,19]. In contrast, contradictory evidence exists where bulky fabric architectures and vacuum-induced dry spots resulted in poor fiber wetting and localized void content [18], which improved the transverse tensile strength and interlaminar shear strength compared to VARTM [19]. These contradictory trends directly affect the longitudinal-transverse contrast, yet the anisotropy was not evaluated.

Although reported improvements are often expressed as absolute gains, the structural performance of unidirectional composites is governed not only by the magnitudes of the individual properties but also by the directional relationships among them. Despite extensive research on the manufacturing-induced variations in mechanical properties, the effect of the manufacturing process on the anisotropic mechanical response remains poorly understood. It is well understood that the manufacturing process alters fiber volume fraction, resin uniformity, fiber alignment, and void content. But this, in turn, modifies the relative balance among longitudinal, transverse, bending, and shear load-carrying mechanisms. Two laminates that

exhibit similar improvements in absolute properties may exhibit different directional mechanical behavior and structural efficiency.

The critical knowledge gap is that, while prior work reports absolute changes in isolated constitutive parameters, it rarely interprets these process-driven variations in terms of their influence on anisotropic mechanical response under multiaxial loading conditions. Furthermore, existing studies rarely quantify directional dependency using anisotropy metrics. While a few studies explored the directional dependency across alternative structural mediums such as aramid/nylon knitted composites [20] and polyurethane foams [21], Hamanaka et al. [22] evaluated the flexural anisotropy of glass fibers using longitudinal-to-transverse flexural modulus and found that the anisotropy increases linearly with glass fiber content up to 50%. However, these studies focus on material architecture rather than on the evolution of manufacturing-induced anisotropy.

Accordingly, the primary objective of this study is to investigate the evolution of process-induced anisotropy in unidirectional CFRP, GFRP, and BFRP laminates manufactured using HLU and VARTM. Unlike previous studies that focus predominantly on individual mechanical properties, the present work systematically quantifies the degrees of anisotropy derived from tensile and compressive responses, as well as the flexural and interlaminar shear translational indices. By correlating experimentally determined fiber volume fraction and void content with multiaxial mechanical properties, the study establishes a process-structure-anisotropy relationship that links manufacturing-induced microstructural variations to directional mechanical performance. As automotive composite structures are subjected to combined tensile, compression, bending, and shear loading, understanding the effect of the manufacturing process on anisotropy evolution is vital for translating constitutive-level improvements into reliable structural performance.

2. Materials and manufacturing

2.1. Materials

High-performance unidirectional fibers, including carbon, E-glass, and basalt, are used as the primary reinforcements in this study. The matrix system consists of a commercial-grade thermosetting bisphenol A diglycidyl ether (DGEBA) epoxy resin (Araldite® LY 556) paired with an aliphatic amine hardener (HY 951), both procured from Herenba Pvt. Ltd., Chennai, India. A strict stoichiometric resin-to-hardener weight ratio of 100:10 is maintained across all

fabrications, as recommended by the manufacturer. The physical and mechanical properties of the fibers and resin are listed in **Table 1** [25,26].

Table 1. Physical and mechanical properties of fibers and resin

Property	Carbon	E-glass	Basalt	Epoxy LY556
Density (g/cm^3)	1.76	2.54	2.67	1.2
Areal weight (GSM)	400	400	380	-
Ply thickness (mm)	0.4	0.4	0.38	-
Tensile strength (MPa)	4900	2450	2850	52
Tensile modulus (GPa)	230	80	90	3.2
Elongation at break (%)	1.5	2.5	3.15	6

2.2. Manufacturing Methods

Composite laminates measuring 400 × 400 mm are manufactured for each fiber type using two distinct manufacturing methods: HLU and VARTM. For tensile, in-plane shear, compressive, and flexural characterization, the laminates are manufactured to yield a thickness of 1-2 mm. For the interlaminar shear testing, the ply count is increased for the final laminate thickness of 4 mm. All laminates are reinforced with a principal fiber orientation (0°) and designed for a nominal fiber volume fraction of approximately 50%, which is experimentally verified in subsequent sections.

2.2.1. Hand Layup Process

A schematic representation of the open-mold hand layup process is shown in **Fig. 1**. The resin-hardener system is thoroughly mixed under ambient conditions, followed by vacuum degassing to minimize air entrapment. To facilitate demolding, the mold surface is coated with a thin film of hydraulic oil, and a thin plastic sheet is placed over it. A thin resin layer is coated before the first fiber layer is placed, and the fibers are gently hand-pressed to promote impregnation. Air bubbles are removed using manual rolling and gentle pressing. This process is repeated until all the plies are impregnated with resin. Upon completion, a mild steel plate is secured on the mold to apply uniform compaction pressure, promoting consistent fiber compaction and laminate consolidation. The assembly is left to cure for 24 h at 36 °C, followed by a post-curing for 5 h at 100 °C in an air oven.

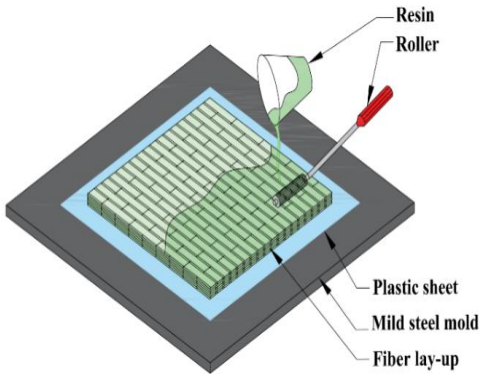


Fig. 1. Schematic representation of the hand layup process

2.2.2. Vacuum-Assisted Resin Transfer Molding Process

The experimental setup for the VARTM process is schematically shown in **Fig. 2**. A 12 mm-thick acrylic plate serves as the mold surface, which is cleaned with acetone to remove contaminants and coated with mold-release wax to facilitate demolding and achieve a smooth finish. Dry fibers are stacked on the mold surface and sequentially covered with a peel ply, infusion mesh, and vacuum bagging film. The perimeter is sealed using sealant tape. A vacuum pump is engaged to apply a continuous negative pressure of -97 kPa (relative) to remove the residual air and apply a uniform consolidation pressure. Resin is introduced under vacuum, ensuring full wet-out through the fiber layers and promoting complete impregnation. After infusion, the laminate remains under vacuum during curing (24 h at 36 °C), followed by post-curing at 100 °C for 5 h in an air oven.

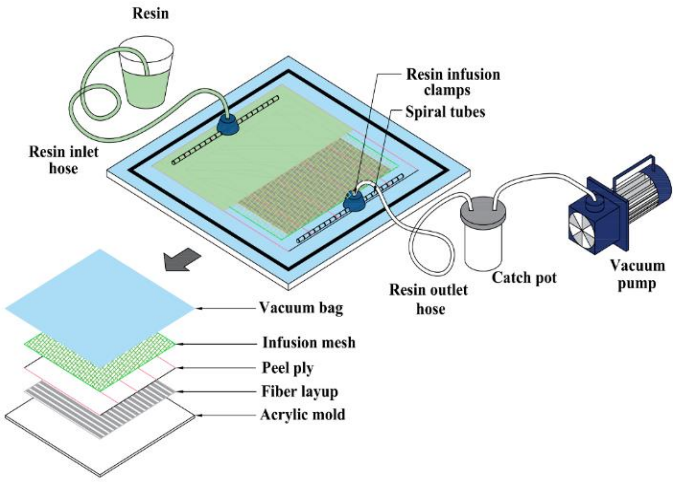


Fig. 2. Schematic representation of the VARTM process

3. Experimental Methods

This section provides a brief description of the experimental configurations and analytical formulations utilized to determine the bulk physical properties (density, fiber volume fraction, and void content) and the multiaxial mechanical properties of the composite laminates. All tests are conducted in accordance with ASTM standards. Furthermore, the procedures for evaluating anisotropy indices and for statistical analysis are also explained in detail.

3.1. Density, Fiber Volume, and Void Fraction Analysis

Experimental bulk density is determined using ASTM D792 [25]. Each specimen is weighed first in ambient air and subsequently in fully immersed distilled water. The reduction in apparent weight corresponds to the volume of displaced liquid. The composite density is calculated using Eqn. 1.

$$\rho_c = \left[\frac{W_{air}}{W_{air} - W_{water}}\right] \times \rho_{water} \quad (1)$$

where, ρ_c and ρ_{water} represent the densities of the composite and water (g/cm³), respectively, W_{air} and W_{water} represent the specimen weight in air and in water (g).

The experimental density is benchmarked against the theoretical composite density, calculated using the rule–of–mixtures formulation in Eqn. 2:

$$\rho_{tc} = V_f \rho_f + (1 - V_f)\rho_m \quad (2)$$

where ρ_{tc} is the theoretical density (g/cm³), V_f is the nominal fiber volume fraction (0.50), ρ_f and ρ_m are the constituent densities (g/cm³) of the fiber and resin, respectively. The percentage deviation ($\Delta\rho$) from the theoretical density is computed using Eqn. 3,

$$\Delta\rho = \left(\frac{\rho_c - \rho_{tc}}{\rho_{tc}}\right) \times 100 \quad (3)$$

The matrix acid digestion method (ASTM D3171 Procedure A: matrix digestion using nitric acid) is used to determine the fiber volume fractions and void content [26]. Specimens measuring 50 × 10 mm are cut from three regions of the laminate, weighed, and subsequently immersed in concentrated nitric acid (69%–72%) at 80 ºC, inside a laboratory fume hood for 5 h. The solution is filtered, and digestion is repeated until the matrix is completely degraded. Following full matrix degradation, the fibers are filtered, rinsed twice with water and acetone, dried, and weighed. The final fiber volume fraction (V_F) and volumetric void fraction (V_V) are calculated based on Eqns. 4 and 5,

$$V_F = \left[\frac{W_f/\rho_f}{W_c/\rho_c}\right] \times 100 \quad (4)$$

$$V_V = \left[1 - \frac{(W_f/\rho_f) + ((W_c - W_f)/\rho_m)}{(W_c/\rho_c)}\right] \times 100 \quad (5)$$

where W_c and W_f are the weights of the composite and fibers (g), respectively.

3.2. Mechanical Testing

The composite laminates are characterized for their mechanical properties, including tensile, compression, in-plane shear, flexural, and interlaminar shear tests. The corresponding specimen designations are summarized in **Table 2**. Three samples are tested for each specimen, and the average values with standard deviations are mentioned.

3.2.1.Tensile Characterization

Uniaxial tensile tests are performed according to ASTM D3039 [27] along both the longitudinal (0°) and transverse (90°) fiber direction to determine the respective moduli (E_{T1} and E_{T2}), ultimate tensile strengths (X_T and Y_T), and failure strains (ϵ_{1T} and ϵ_{2T}). Tests are conducted on a 100 kN universal testing machine (UTM), at a displacement rate of 2 mm/min. The gauge length of the specimens for longitudinal and transverse tensile tests is 150 mm and 75 mm, respectively, with a grip zone length of 50 mm. Aluminum end-tabs (3 mm thick) are bonded to prevent slippage and breakage.

To benchmark the experimental longitudinal and transverse tensile moduli, analytical modeling is carried out on two distinct models:

- *Idealized baseline model:* Assumes laminates with a fiber volume fraction of 50% (V_f =0.50) and no voids. The baseline longitudinal and transverse properties are calculated using the classical rule-of-mixtures (ROM) equations (Eqns 6 and 7):

$$(E_{T1})_{base} = V_f E_f + (1 - V_f) E_f \quad (6)$$

$$(E_{T2})_{base} = \frac{E_f E_m}{V_f E_m + (1 - V_f) E_f} \quad (7)$$

where $(E_{T1})_{base}$ and $(E_{T2})_{base}$ are the baseline longitudinal and transverse tensile moduli (GPa), respectively, E_f and E_m are the tensile moduli of fiber and resin (GPa), respectively.

- *Composition-corrected model:* Introduces the experimentally determined fiber, resin, and void fractions. The corrected properties are calculated using Eqns. 8-11,

$$V_{f_corr} = \frac{V_F}{100 - V_V} \tag{8}$$

$$V_{m_corr} = \frac{100 - V_F - V_V}{100 - V_V} \tag{9}$$

$$E_{T1_corr} = V_{f_corr}E_f + V_{m_corr}E_m \tag{10}$$

$$E_{T2_corr} = \frac{E_f E_m}{V_{f_corr}E_f + V_{m_corr}E_m} \tag{11}$$

where V_{f_corr} and V_{m_corr} are the composition-corrected fiber volume and resin fractions, respectively, E_{T1_corr} and E_{T2_corr} are the composition-corrected longitudinal and transverse tensile moduli (GPa), respectively.

Table 2. Specimen designations for different fiber types, orientations, and manufacturing processes

Test	HLU			VARTM		
	CFRP	GFRP	BFRP	CFRP	GFRP	BFRP
Tensile-0°	H-C-T0	H-G-T0	H-B-T0	V-C-T0	V-G-T0	V-B-T0
Tensile-90°	H-C-T90	H-G-T90	H-B-T90	V-C-T90	V-G-T90	V-B-T90
Tensile-45°	H-C-T45	H-G-T45	H-B-T45	V-C-T45	V-G-T45	V-B-T45
Compression-0°	H-C-C0	H-G-C0	H-B-C0	V-C-C0	V-G-C0	V-B-C0
Compression-90°	H-C-C90	H-G-C90	H-B-C90	V-C-C90	V-G-C90	V-B-C90
Flexural	H-C-F	H-G-F	H-B-F	V-C-F	V-G-F	V-B-F
ILSS	H-C-ILSS	H-G-ILSS	H-B-ILSS	V-C-ILSS	V-G-ILSS	V-B-ILSS

Abbreviations: H=Hand lay-up; V=VARTM, C=Carbon; G=Glass; B=Basalt; T=Tensile; C=Compression; F=Flexural; ILSS=Short beam

3.2.1.1. In-Plane Shear Characterization

The in-plane shear modulus (G_{12}) is evaluated using an off-axis tensile test of balanced $[\pm 45°]_{ns}$ symmetric laminates in compliance with ASTM D3518 [28]. The specimen maintained an active gauge length of 175 mm and a 50 mm grip length on each side. The in-plane shear modulus is directly obtained from the slope of the linear-elastic chord region of the stress-strain response using Eqn. 12 in accordance with the standard:

$$G_{12} = \frac{\Delta\tau_{12}}{\Delta\gamma_{12}} \tag{12}$$

where $\Delta\tau_{12}$ is the difference in applied shear stress between two shear points (MPa), and $\Delta\gamma_{12}$ is the difference between the two shear strain points. The maximum shear stress S_{12} is calculated using Eqn. 13:

$$S_{12} = \frac{P^m}{2AS} \tag{13}$$

where P^m is the maximum shear stress (N), and A is the cross-sectional area (mm^2) in accordance with ASTM D3039.

3.2.2. Compression Characterization

Uniaxial compression tests are performed according to ASTM D3410 [29] to determine the longitudinal and transverse compression moduli (E_{C1} and E_{C2}), ultimate tensile strengths (X_C and Y_C), and failure strains (ϵ_{1C} and ϵ_{2C}). While the combined loading framework of ASTM D6641 [30] is generally recommended, ASTM D3410 was adopted due to resource limitations. Both longitudinal and transverse testing utilized gauge and grip lengths of 40 mm. The UTM is operated at a continuous crosshead displacement rate of 1.5 mm/min, with a hydraulic gripping pressure of 3.5 MPa to prevent slipping.

3.2.3. Flexural Characterization

Flexural properties are evaluated using a three-point bending test in accordance with ASTM D7264 [31], with a displacement rate of 1 mm/min. The support span length (L) is set to 100 mm with an overhanging length of 30 mm, and a support-to-thickness ratio of 40:1. The flexural modulus (E_F), flexural strength (σ_F), and failure strain (ϵ_F) are calculated using Eqns. 13-15:

$$E_F = \frac{mL^3}{4bh^3} \tag{13}$$

$$\sigma_F = \frac{3PL}{2bh^2} \tag{14}$$

$$\varepsilon_F = \frac{6\delta d}{L^2} \tag{15}$$

where m is the initial slope of the linear region in the load-displacement curve (N/mm), P is the peak load (N), and δ is the mid-span deflection (mm), h and b are the specimen thickness and width (mm), respectively.

246 *3.2.4. Interlaminar Shear Strength (ILSS) Characterization*

247 Interlaminar shear strength (τ_{ILSS}) is calculated using the short beam test conducted in
248 accordance with ASTM D2344 [32] under a three-point bending fixture at a crosshead
249 displacement rate of 1 mm/min. The specimen length-to-thickness and width-to-thickness
250 ratios are taken as 6.0 and 2.0, respectively, to preserve shear-dominant failure. The loading
251 roller diameter is set to 6 mm, and the twin support roller diameter is 3 mm. The test is
252 terminated once the loading roller travels exceeds the overall specimen thickness or upon a
253 significant drop in the applied load. The ultimate interlaminar shear capacity is computed using
254 Eqn. 16:

$$\tau_{ILSS} = \frac{0.75P_{max}}{bh} \tag{16}$$

255 where P_{max} is the peak force sustained before delamination failure (N).

256 **3.3. Anisotropy Analysis**

257 The macroscopic directional dependency of the processed unidirectional plates is
258 systematically evaluated by introducing normalized mechanical modulus and strength ratios
259 derived from the experimental datasets. The calculated anisotropy indices isolate how process-
260 induced architectural deviations affect mechanical performance under multiaxial loading.

261 *3.3.1. Tensile Degree of Anisotropy*

262 The classical tensile degrees of anisotropy represent the directional disparity between the
263 principal longitudinal and transverse properties (longitudinal-to-transverse stiffness (DA_{ET})
264 and strength ($DA_{\sigma T}$) ratios) and between longitudinal and in-plane shear stiffness (DA_{G12}).
265 The metrics are calculated using Eqns. 17-19, following Daniel et al. [33]:

$$DA_{ET} = \frac{E_{T1}}{E_{T2}} \tag{17}$$

$$DA_{G12} = \frac{E_{T1}}{G_{12}} \tag{18}$$

$$DA_{\sigma T} = \frac{X_T}{Y_T} \tag{19}$$

266 Higher DA values indicate a highly directionally sensitive, fiber-dominant material response,
267 whereas DA demonstrates improved isotropy due to better fiber-resin interfacial bonding and
268 load transfer.

3.3.2. Compression Anisotropy Indices

The concept of anisotropy is extended to compression loading through compression anisotropy indices (AI) (compression modulus (AI_{EC}) and strength ($AI_{\sigma C}$) ratios), and are calculated using Eqns. 20 and 21:

$$AI_{EC} = \frac{E_{C1}}{E_{C2}} \tag{20}$$

$$AI_{\sigma C} = \frac{X_C}{Y_C} \tag{21}$$

3.3.3. Flexural and Interlaminar Shear Translational Indices

The DA is further generalized to out-of-plane responses, flexural (modulus (AI_{EF}) and strength ($AI_{\sigma F}$)) and interlaminar shear translational indices (AI_{ILSS}), and are calculated based on Eqns. 22-24:

$$AI_{EF} = \frac{E_{T1}}{E_F} \tag{22}$$

$$AI_{\sigma F} = \frac{X_T}{\sigma_F} \tag{23}$$

$$AI_{ILSS} = \frac{X_T}{\tau_{ILSS}} \tag{24}$$

The flexural indices represent the efficiency of modulus and strength translation from tensile to bending, while the interlaminar shear index determines the tensile–shear efficiency.

3.4. Statistical Evaluation

A two-way ANOVA is used to statistically evaluate the influence of manufacturing method (Factor A: HLU vs VARTM), and fiber type (Factor B: Carbon vs E-glass vs Basalt). The degrees of freedom are set to (1,12) for Factor A and (2,12) for both Factor B and the coupled interaction term (A × B), with critical F-values of 4.75 and 3.89, respectively. The Kolmogorov-Smirnov and Brown-Forsythe tests confirm normality and homogeneity of variance, validating the analysis at a p-value of 0.05 for comparing the influence of manufacturing and fiber.

4. Results and Discussion

This section presents the effects of the manufacturing process on the bulk physical characteristics (density, fiber volume fraction, and void content), the mechanical properties, and the anisotropy behavior of the composite laminates. Furthermore, a brief statistical

evaluation using a two-way ANOVA is provided, highlighting the statistical significance of the effects of fiber type, manufacturing method, and the coupled process-fiber interactions.

4.1. Density, Fiber Volume, and Void Fraction Analysis

The experimentally determined densities, fiber volume fractions, and void volume contents for are summarized in the supplementary file (Tables S1 and S2). A comparative overview shows that VARTM laminates exhibit slightly higher densities than HLU laminates, with higher fiber volume fractions and lower void contents. Specifically, the measured densities (g/cm^3) for VARTM are 1.47 (CFRP), 1.80 (GFRP), and 1.92 (BFRP) compared to 1.41, 1.61, and 1.69, respectively, for HLU. Since fiber density exceeds resin density, higher fiber volume fractions result in an overall increase in laminate density [12].

A comparative analysis of the measured density with the rule-of-mixtures-predicted densities is presented in Table S3 of the supplementary file. The VARTM laminates closely match theoretical values, with minimal percentage deviations ($\Delta\rho \approx$ -0.47% to -3.64%), indicating effective laminate compaction, higher fiber packing efficiency, and minimal void content. In contrast, HLU laminates exhibit greater deviations ($\Delta \approx$ -4.53% to -13.85%), reflecting lower fiber volume fraction and increased void entrapment due to manual layup variability. The measured densities across all fibers remain within physically consistent limits, validating their suitability for mechanical characterization. To achieve uniform mechanical performance, these deviations must be minimized, as severe physical non-uniformity can introduce local stiffness variations and premature failure initiation under multiaxial loading conditions.

As illustrated in **Fig. 3**, the fiber, resin, and void fractions distinctly differentiate the consolidation efficiency and constituent distribution achieved by the two manufacturing processes. The vacuum-driven pressure gradient in VARTM applies a continuous, uniform atmospheric consolidation force that maximizes dry preform compaction before and during resin infiltration. This systematic extraction of residual air pockets results in achieving a final volumetric void fraction below 2% cross all VARTM configurations. In contrast, HLU relies on manual resin application and static top-plate weighting, resulting in higher resin content and greater void entrapment than the corresponding VARTM laminates.

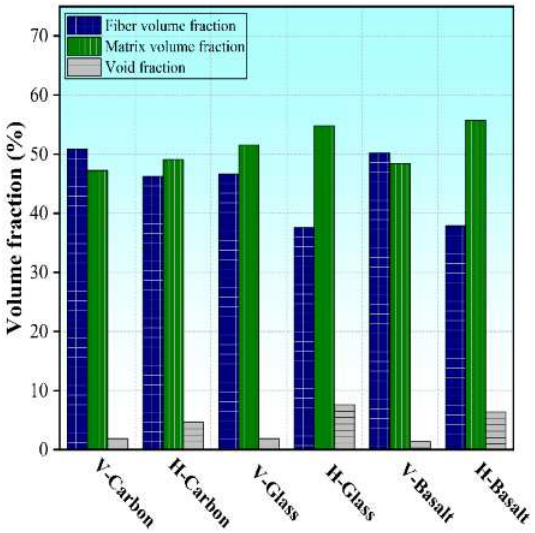


Fig. 3. Fiber, matrix, and void fractions in laminates produced by HLU and VARTM

Among the distinctive fiber types, the HLU-based GFRP exhibits the lowest absolute fiber volume fraction, attributing to the high initial bulk thickness and unique compliance of woven E-glass fabric, which absorbs an excessive volume of liquid matrix while resisting uniform fabric compaction under manual pressure, which closely aligns with the findings of Dorigato et al. [34]. Interestingly, BFRP exhibits a slightly higher fiber volume fraction and lower void volume than the GFRP counterparts under identical processing conditions. This trend is consistent with the findings of Rafat et al. [36], suggesting that the higher bulk density and improved resin permeability of basalt fibers accelerate resin impregnation compared to glass fibers, even under manual processing.

The target composition of ~50% fiber and ~50% resin volume represents an optimized laminate with minimal voids. The HLU laminates deviate significantly from this optimized target, particularly for GFRP and BFRP configurations, highlighting the difficulty of achieving uniform resin control and fiber compaction in manual layup. Conversely, the closed-loop VARTM laminates closely approach or slightly exceed the target, particularly with CFRP and BFRP, achieving fiber-rich laminates with void fractions below 2%. These process-driven physical and microstructural characteristics provide a fundamental explanation for the distinct changes in multiaxial mechanical behavior, stiffness, strength, and statistical reproducibility. Overall, these results confirm that VARTM produces structurally efficient laminates with superior consolidation and minimal defects, providing a more reliable foundation for multiaxial mechanical performance.

4.2. Mechanical Characterization

The samples manufactured using VARTM and HLU are tested under multiaxial loading conditions, including longitudinal and transverse tension, in-plane shear, longitudinal and transverse compression, flexural, and interlaminar shear. The corresponding stress-strain curves are presented, along with embedded fracture images, to directly correlate the mechanical response with the observed failure mechanisms.

4.2.1. Tensile and In-Plane Shear Performance

This subsection compares the tensile performance of unidirectional composites, including longitudinal and transverse tensile and in-plane shear constitutive behavior, using the stress-strain responses in **Fig. 4-6**. **Table 3** summarizes the average tensile and in-plane shear properties, highlighting the effect of fiber volume fraction and void content on mechanical behavior.

4.2.1.1. Longitudinal and Transverse Tensile Responses

Under longitudinal tensile loading (**Fig. 4a-c**), all composite laminates exhibit an initial linear-elastic response followed by catastrophic brittle failure without significant plastic deformation. The VARTM laminates exhibit a steeper elastic slope and higher tensile modulus and strength than their HLU counterparts. At failure, the VARTM laminates predominantly exhibit longitudinal splitting within the gauge section (classified as SGM failure). Conversely, HLU showed a more gradual post-peak stress degradation, suggesting a more progressive failure process than the abrupt failure observed in VARTM laminates.

Quantitatively, VARTM processing increases longitudinal modulus and strength 36.1% and 85.3% for CFRP, 58.6% and 167.9% for GFRP, and 35.2% and 27.7% for BFRP, respectively. Elongation at break also improves with increases of 25.7% (CFRP), 106.7% (GFRP), and 11.1% (BFRP). This increase in mechanical efficiency is consistent with the superior fiber volume fractions and lower void content, achieved through continuous vacuum compaction [11]. The magnitude of improvement, however, varies among the reinforcement systems, with GFRP exhibiting the strongest sensitivity to the manufacturing route, followed by CFRP and BFRP. In contrast, improvements in GFRP and BFRP indicate that the effect of the manufacturing process varies substantially among the reinforcement systems. The high tensile stiffness and predictable fiber-dominant failure modes demonstrate the effectiveness of VARTM in improving the overall longitudinal tensile response across all three composite systems.

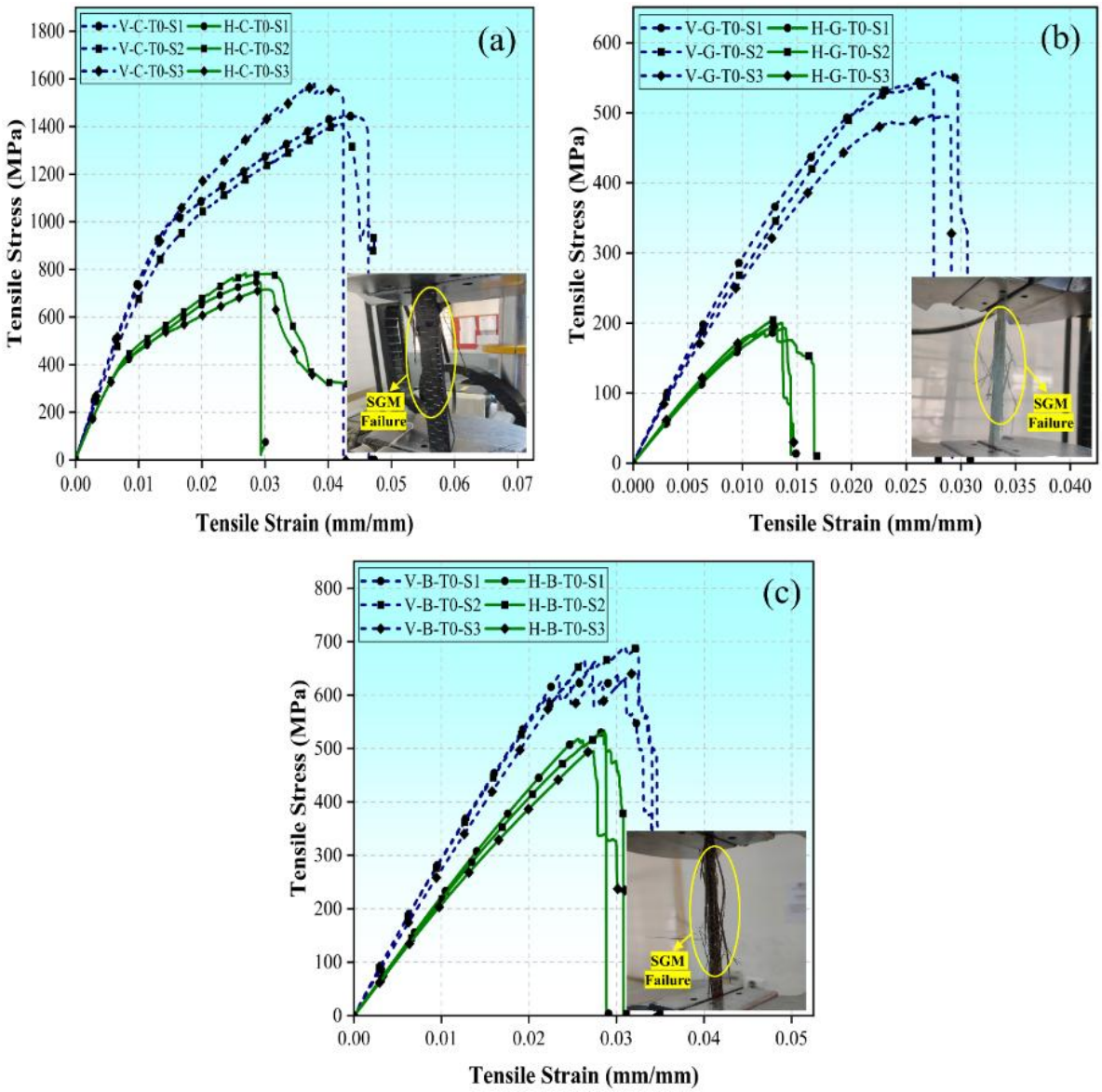


Fig. 4. Stress-strain relationship of (a) CFRP, (b) GFRP, and (c) BFRP tested under longitudinal tensile loading

Under transverse tensile loading (**Fig. 5a-c**), the mechanical response transitions to matrix-dominant and interface-sensitive. VARTM laminates exhibit smoother, more continuous stress-strain responses, reaching higher stresses and strains before failure. Conversely, HLU laminates display earlier deviation from linearity and reduced failure strains relative to the corresponding VARTM laminates. Both laminates display brittle failure, typically by lateral gauge-mid splitting (LGM). Quantitatively, VARTM enhances the transverse modulus and strength by 19.6% and 29.4% for CFRP, 27.4% and 79.5% for GFRP, and 64.3% and 18.7% for BFRP, respectively. The substantially larger improvements observed in GFRP and BFRP suggest that transverse, matrix-dominant responses are more strongly influenced by manufacturing process than longitudinal fiber-dominant responses. VARTM process-induced enhancements differ

from those reported by Scalici et al. [19], who found that vacuum infusion of basalt fibers often leads to localized dry spots, underscoring the need for process optimization.

Elongation at break also increases by 13.3% for CFRP, 86.6% for GFRP, and 2.6% for BFRP. The relatively minor improvement in BFRP failure strain suggests that the transverse deformation of basalt laminates is governed by inherently strong fiber-resin interfacial bonding rather than process-induced variations as observed in CFRP and GFRP laminates [35]. Overall, the findings confirm that VARTM processing consistently enhances stiffness, strength, and ductility across all laminate systems, with higher fiber volume fraction, reduced voids, and strong interfacial bonding [36].

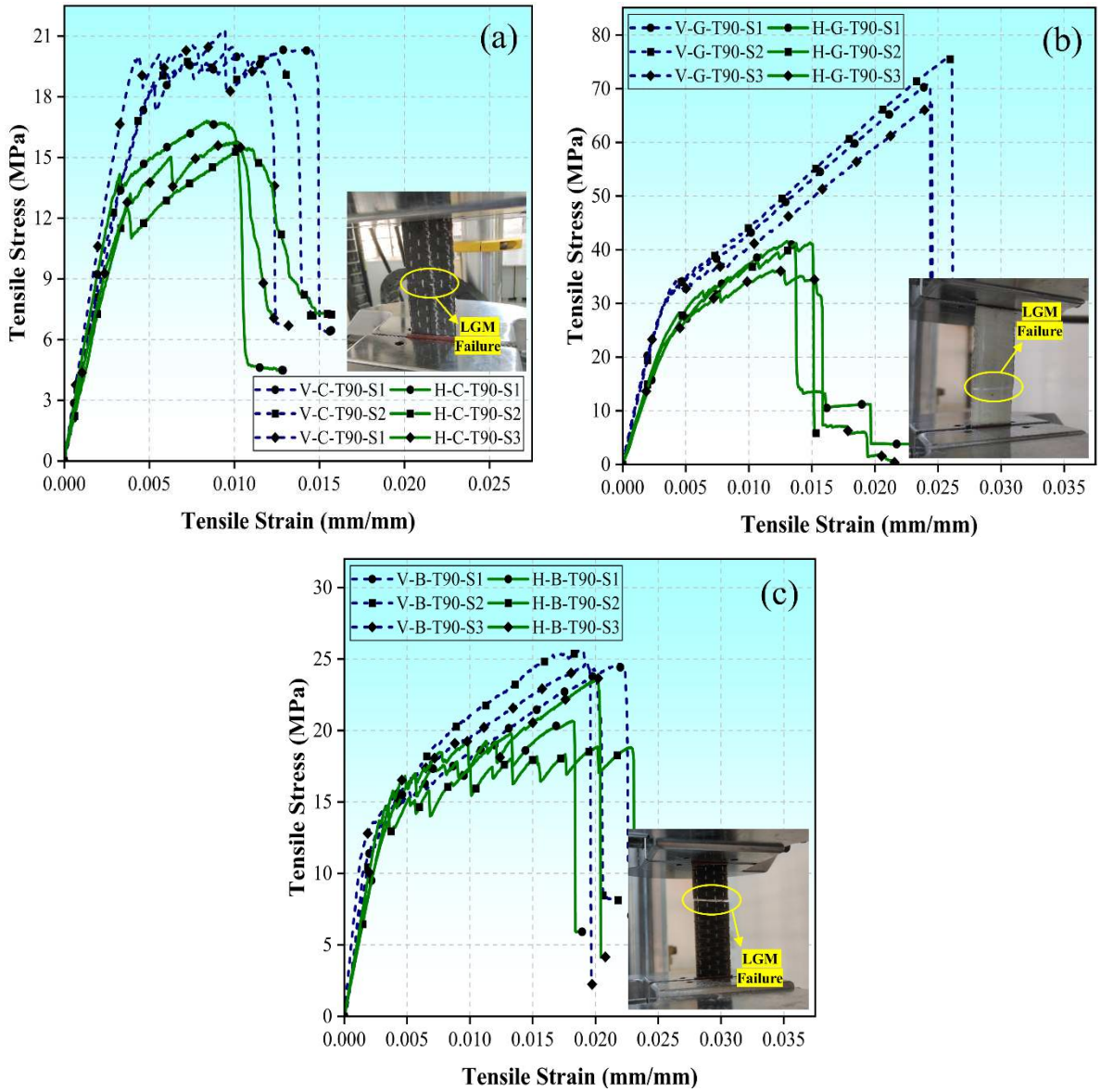
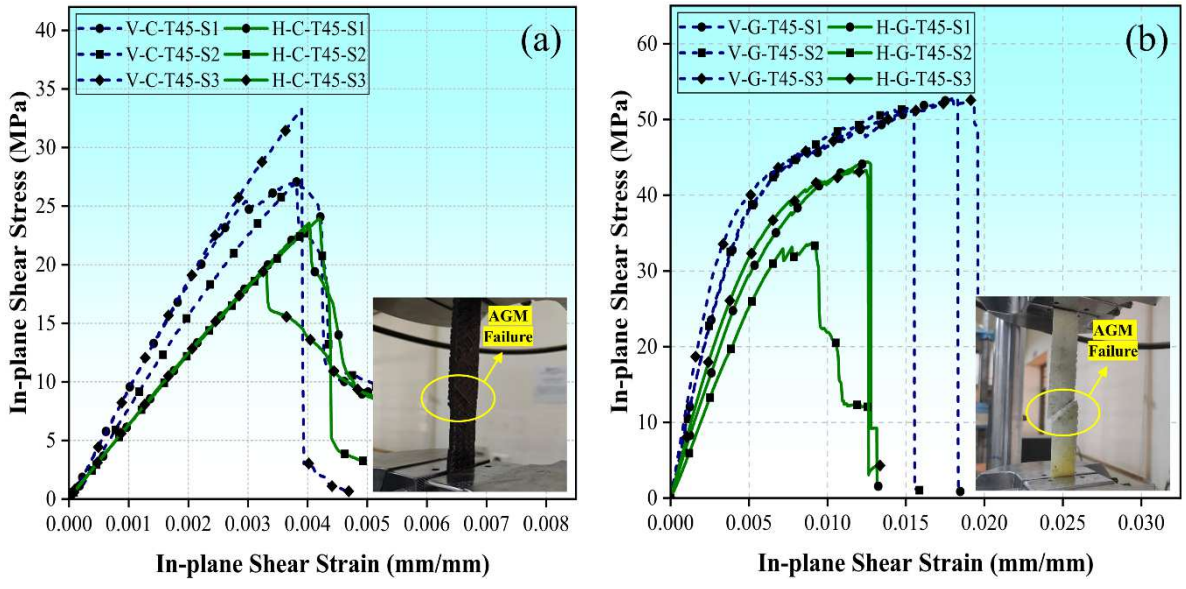


Fig. 5. Stress-strain relationship of (a) CFRP, (b) GFRP, and (c) BFRP tested under transverse tensile loading

4.2.1.2. In-Plane Shear Responses

The off-axis in-plane shear stress-strain relationship and corresponding failure morphologies are presented in **Fig. 6a-c**. All laminates exhibit brittle failure through angled splitting along the primary fiber axes at the gauge section (AGM). HLU laminates exhibit premature load drops and greater fluctuations in the stress-strain response before failure. In contrast, the VARTM laminates exhibit a well-defined linear elastic region, gradual load transfer, and fewer premature or catastrophic load drops, resulting in a more consistent shear response during loading. VARTM consistently enhances the in-plane shear properties of CFRP and GFRP. For CFRP, the shear modulus and strength increase by 35.9% and 30.3%, while GFRP shows improvements by 44.5% and 29.7%, respectively. Interestingly, BFRP displays a slightly deviated trend: VARTM increases shear modulus by 17.9%, while HLU exhibits a marginal increase of 6.7% in shear strength, highlighting fiber-specific interactions with resin and process defects. The contrasting behavior between different fiber types underscores that increases in stiffness do not necessarily translate into proportional increases in ultimate shear strength, particularly in basalt-fiber laminates.

Elongation at break further emphasizes the influence of the manufacturing process. For CFRP, elongation is nearly identical under both methods, with HLU showing a marginal 5% increase. GFRP shows a 55.8% increase with VARTM, while BFRP exhibits slightly higher ductility in HLU (12.6%). Elnekhaily et al. [37] explained that the higher elongation at break observed in HLU GFRP and BFRP is likely due to the non-uniform void distribution in the HLU process, which causes localized stress concentration. As voids coalesce, stress is redistributed nonlinearly, allowing additional energy dissipation before final failure.



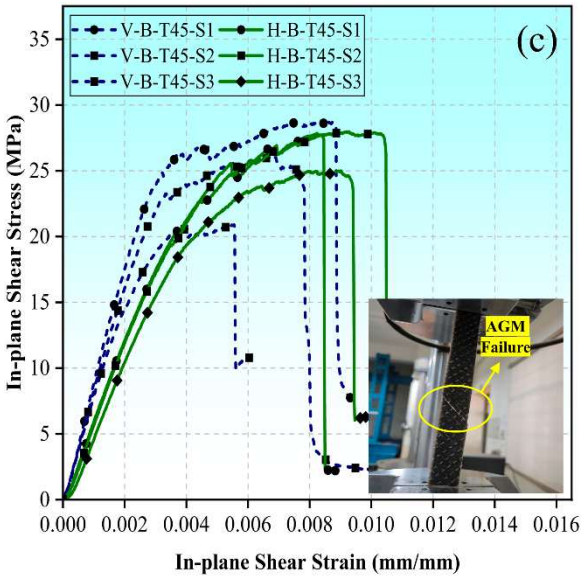


Fig. 6. Stress-strain relationship of (a) CFRP, (b) GFRP, and (c) BFRP tested under in-plane shear loading

412 **Table 3**. Average tensile and in-plane shear properties of unidirectional composite laminates
413 manufactured by HLU and VARTM

Properties	Symbol (unit)	HLU			VARTM		
		CFRP	GFRP	BFRP	CFRP	GFRP	BFRP
Longitudinal tensile modulus	E_{T1} (GPa)	58.41± (0.31%)	19.21± (3.70%)	22.25± (3.11%)	79.5 ± (4.34%)	30.47± (4.05%)	30.08± (4.92%)
Transverse tensile modulus	E_{T2} (GPa)	3.68± (12.27%)	6.86± (5.32%)	4.79± (5.98%)	4.40± (10.91%)	8.74± (1.86%)	7.87± (7.23%)
In-plane shear modulus	G_{12} (GPa)	5.87± (1.09%)	6.16± (12.02%)	5.65± (3.49%)	7.98± (8.94%)	8.90± (8.79%)	6.66± (16.00%)
Longitudinal tensile strength	X_T (MPa)	797.22± (4.43%)	198.79± (2.75%)	519.48± (3.92%)	1476.88± (6.08%)	532.72± (6.00%)	663.64± (3.68%)
Transverse tensile strength	Y_T (MPa)	15.99± (4.48%)	39.67± (7.67%)	21.04± (11.44%)	20.69± (2.53%)	71.20± (6.11%)	24.97± (2.17%)
In-plane shear strength	S_{12} (MPa)	22.36± (10.56%)	40.39± (14.61%)	26.92± (6.23%)	29.12± (12.28%)	52.39± (1.44%)	25.22± (15.85%)

Note: values represent mean ± standard deviation (%)

4.2.1.3. Analytical Modeling and Rule-of-Mixtures benchmarking

The detailed calculations comparing the experimental longitudinal and transverse tensile moduli against both the idealized baseline ROM and composition-corrected models are compiled in Tables S4 and S5 in the supplementary file. The longitudinal tensile modulus (E_{T1}) generally follows the ROM predictions, as it is primarily governed by fiber stiffness and fiber volume fraction. VARTM laminates exhibit higher gains in composite-corrected moduli compared to HLU, reflecting improved fiber packing, higher fiber volume fraction, and lower void content. However, across all fiber types, the observed 20–50% reduction in experimental E_{T1} relative to the composition-corrected formulation cannot be fully described by constituent fractions alone, and that additional manufacturing-related effects, such as fiber misalignment or fiber waviness, as well as imperfect fiber-resin load transfer, also influence the measured mechanical behavior.

In contrast, the transverse tensile modulus (E_{T2}) is matrix-dominated, governed primarily by matrix stiffness and void distribution. While composition-corrected moduli show only marginal deviations (-21% to +3%) relative to the baseline model, the experimental values exhibit a broader spread (-42% to +42%), underscoring the sensitivity of transverse performance to local manufacturing defects. The significant positive deviations in GFRP may be attributed to the presence of transverse glass fiber knitting threads within the woven architecture, which contribute to the transverse load-carrying response of the laminate. In contrast, the negative deviations in CFRP (-32% for VARTM and -38% for HLU) indicate high sensitivity to transverse properties and manufacturing-related effects that the analytical models do not explicitly capture. The improved transverse properties observed in VARTM BFRP demonstrate that the manufacturing route exerts a measurable influence on the lateral capacity of the laminate. Conversely, the lower transverse properties of the HLU laminates make them more sensitive to processing variability.

Overall, these findings underscore that the longitudinal modulus is relatively insensitive to composite-corrected analytical formulations compared with the transverse modulus, which exhibits substantially larger deviations from theoretical predictions [38], [39]. This behavior indicates the matrix-dominated transverse properties are more sensitive to manufacturing-related effects than fiber-dominated longitudinal properties, highlighting the limitations of simplified analytical models in predicting transverse mechanical response. VARTM process suppresses these vulnerabilities by evenly distributing meso- to micro-void content into the

resin, reducing local stress concentrations and delaying premature failure. Conversely, the hand layup process often introduces larger voids and dry spots due to incomplete fiber wetting, significantly lowering the mechanical properties [12].

4.2.2. Compressive Responses

The compressive constitutive behaviors of the composite laminates along the longitudinal **(Fig. 7a-c)** and transverse **(Fig. 8a-c)** material axes reveal distinct process- and fiber-dependent trends. **Table 4** summarizes the average compressive mechanical properties of laminates manufactured using HLU and VARTM. All laminates exhibit an initial elastic region, followed by brittle brooming failure in the gauge mid (BGM). Under longitudinal compression, the VARTM laminates exhibit a steeper initial elastic region and higher stiffness than HLU. Quantitatively, longitudinal compression modulus increases under VARTM by 45.5% for CFRP, 33.1% for GFRP, and a substantial 431.9% for BFRP, confirming that the fiber–dominated stiffness is strongly influenced by the manufacturing route, with VARTM consistently producing higher longitudinal compressive moduli than HLU.

However, compression strength reveals fiber-dependent trends. While BFRP shows remarkable improvement (240.9%) with VARTM, HLU shows higher strength in CFRP (19.0%) and GFRP (9.3%). Sun et al. [40] noted that the longitudinal compressive failure in CFRP is strongly influenced by fiber micro-buckling and kink-band formation. Although VARTM increased the longitudinal compression stiffness, the CFRP laminates failed at lower compression strain than the corresponding HLU laminates. The lower resin content in VARTM CFRP compared to HLU may have reduced matrix support, leading to premature compression failure at lower compression strength. The relatively smaller difference in longitudinal compression strength of GFRP indicates that the presence of transverse fiber knitting contributed to its compressive stability, thereby reducing the sensitivity to manufacturing method. The contrasting trends in longitudinal compression modulus and strength also suggest that the influence of manufacturing techniques depends strongly on the fiber type.

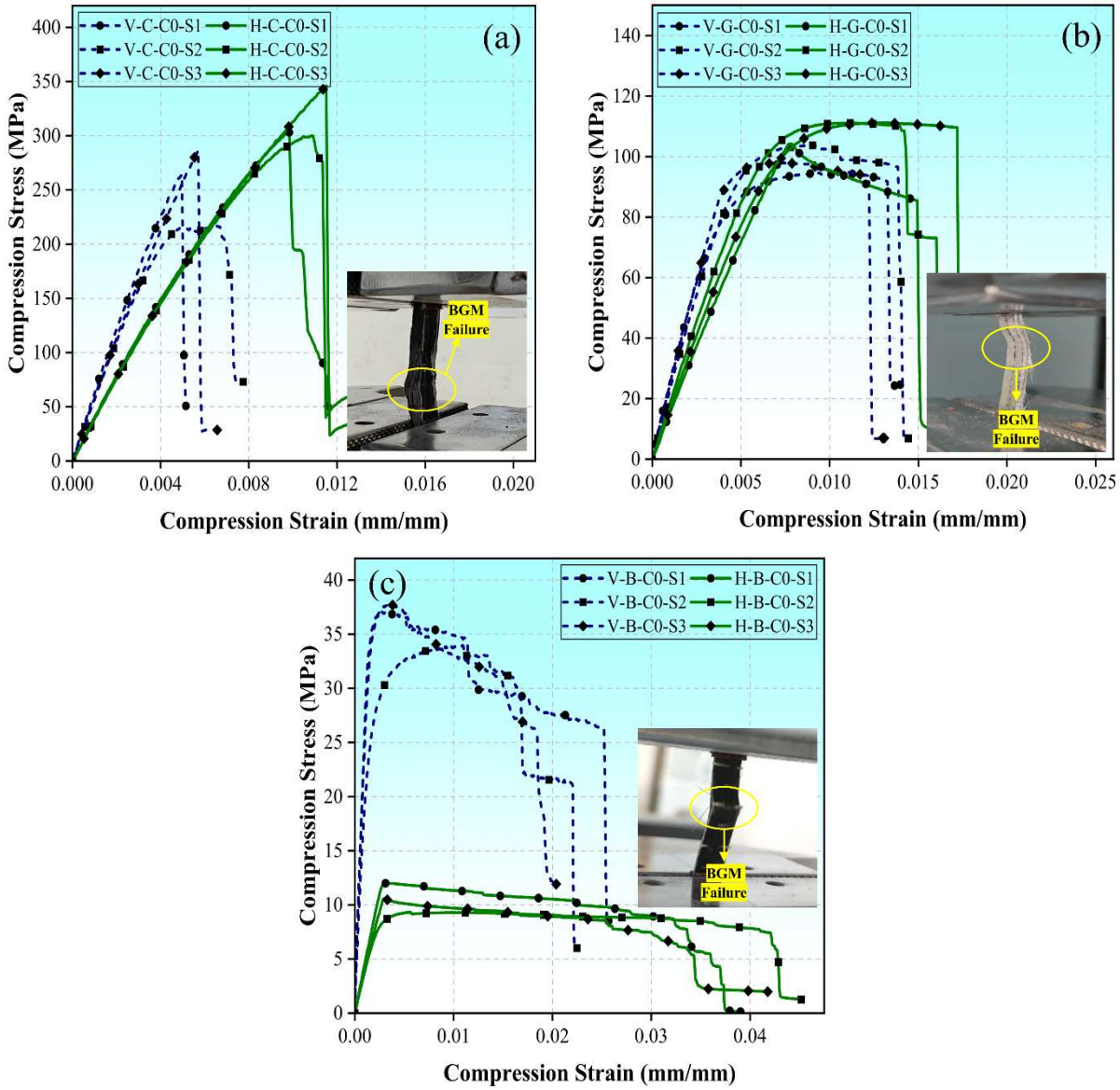


Fig. 7. Stress-strain relationship of (a) CFRP, (b) GFRP, and (c) BFRP tested under longitudinal compression loading

Under transverse compression, VARTM laminates exhibit a steeper linear-elastic response followed by abrupt brittle failure. In contrast, the HLU laminates exhibit a shallower elastic region and extended plastic deformation. VARTM substantially enhances both the transverse compression modulus and strength by 292.7% and 371.7% for GFRP and 150.8% and 143.2% for BFRP. While VARTM improves the modulus by 14.4% for CFRP, the HLU process resulted in a 111.7% increase in strength. The contrasting behavior suggests that the relatively resin-rich composition of HLU CFRP may provide additional lateral support against fiber micro-buckling or kink-band formation, which are the primary compressive failure modes in CFRP and GFRP [40]. Elongation at break follows a similar trend: HLU laminates show higher ductility in CFRP (164.4%) and GFRP (114.8%); VARTM improves ductility modestly in

BFRP, indicating a modest improvement in failure strain relative to the HLU counterpart. Despite their intrinsic toughness, BFRP remains less ductile than GFRP under transverse compression, underscoring the dominant role of resin in transverse mechanical performance. The finding that HLU processing can significantly increase the transverse compressive strength of CFRP demonstrates that maximum fiber compaction achieved in VARTM is not universally beneficial for all loading conditions.

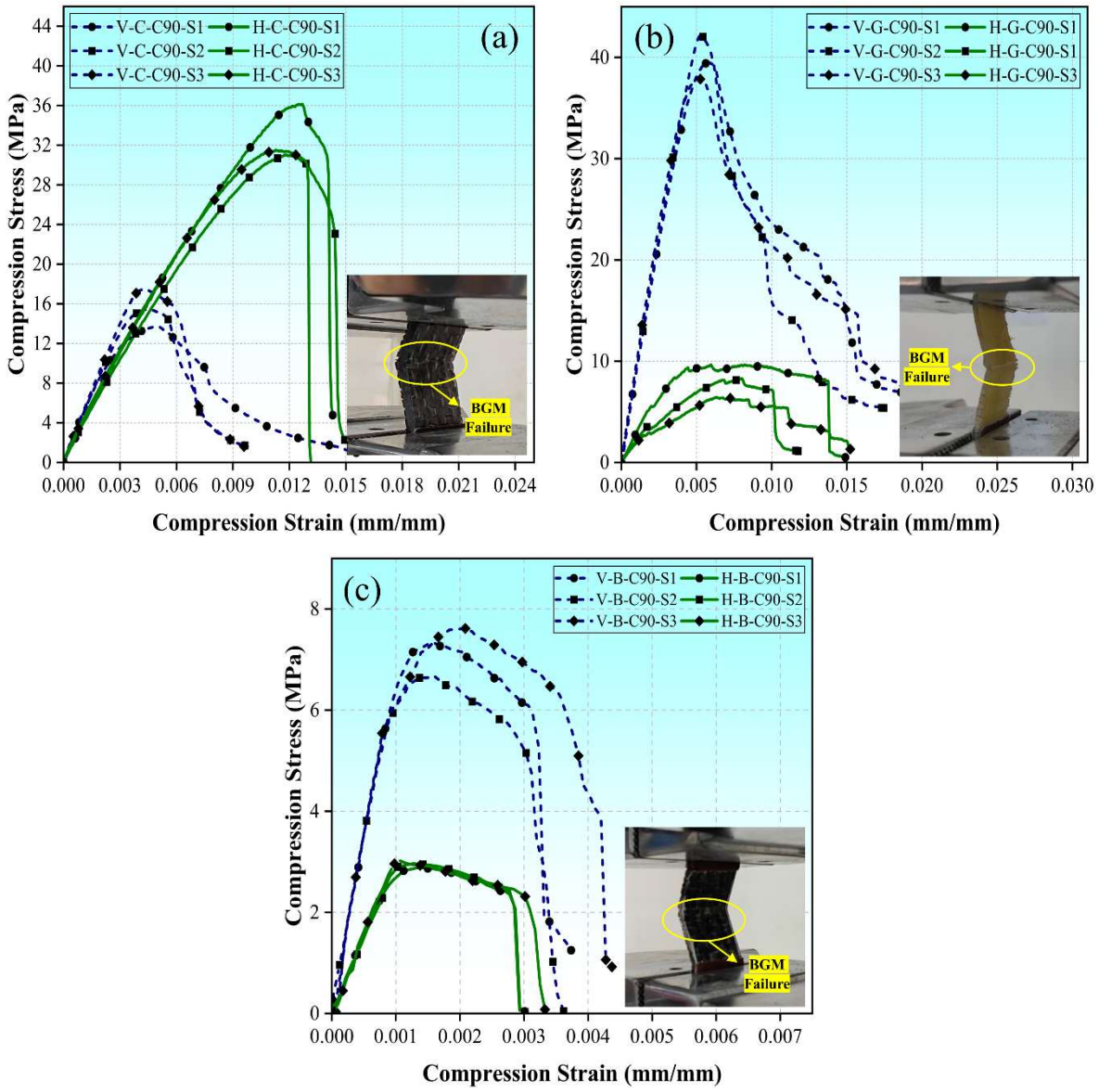


Fig. 8. Stress-strain relationship of (a) CFRP, (b) GFRP, and (c) BFRP tested under transverse compression loading

Table 4. Average compression properties of unidirectional composite laminates manufactured by HLU and VARTM

Properties	Symbol (unit)	HLU			VARTM		
		CFRP	GFRP	BFRP	CFRP	GFRP	BFRP
Longitudinal compression modulus	E_{C1} (GPa)	37.02± (1.33%)	15.9 ± (10.00%)	4.41± (5.00%)	53.8± (6.02%)	21.23± (6.14%)	23.46± (17.74%)
Transverse compression modulus	E_{C2} (GPa)	3.54± (5.64%)	2.48± (18.68%)	3.23± (6.91%)	4.05± (13.80%)	9.74± (3.48%)	8.10± (12.85%)
Longitudinal compression strength	X_C (MPa)	316.06± (8.10%)	108.79± (3.68%)	10.64± (12.69%)	255.91± (13.94%)	98.72± (4.68%)	36.28± (5.68%)
Transverse compression strength	Y_C (MPa)	32.86± (8.58%)	8.44± (10.96%)	2.96± (2.20%)	15.52± (12.15%)	37.91± (5.34%)	7.20± (6.76%)

Note: values represent mean ± standard deviation (%)

4.2.3. Flexural Responses

The flexural response profiles and primary failure behavior of the unidirectional laminates under three-point bending loads are as shown in **Fig. 9a-c**, with the average flexural properties summarized in **Table 5**. The VARTM laminates exhibit steeper initial slopes, followed by abrupt brittle failure at peak load for CFRP and GFRP. This higher flexural stiffness is reflected by the steeper initial load-displacement response exhibited by the VARTM laminates. In contrast, the corresponding HLU laminates exhibit irregular slopes with broader, less-defined peaks and a gradual post-peak load reduction, reflecting a progressive reduction in load-carrying capacity following the peak load.

Quantitatively, VARTM improves flexural modulus and strength of the synthetic fibers compared to HLU. CFRP exhibits 59.4% and 59.6% increases in modulus and strength, respectively, while GFRP shows 60.3% and 6.9% increases. However, BFRP breaks this trend: VARTM increases flexural modulus by 34.6% but reduces flexural strength by 18.4%. Because the three-point bending test induces tensile stress at the bottom layer and compressive stress at the top layer, the lower transverse compressive strength of BFRP significantly reduces its flexural strength, consistent with observations by Scalici et al. [19]. The BFRP results demonstrate that the response to the manufacturing route is highly loading mode-dependent, as the same process that increases stiffness does not necessarily maximize flexural strength. Elongation at break further highlights the stiffness-ductility trade-off: VARTM enhances CFRP

by 8.5%, while HLU laminates show higher values for GFRP (41.81%) and BFRP (81.60%), due to progressive micro-cracking that delays catastrophic failure. Overall, VARTM improves load-carrying capacity across all laminates, whereas HLU induces higher failure strain in GFRP and BFRP, reaffirming the process-dependent balance among stiffness, strength, and ductility.

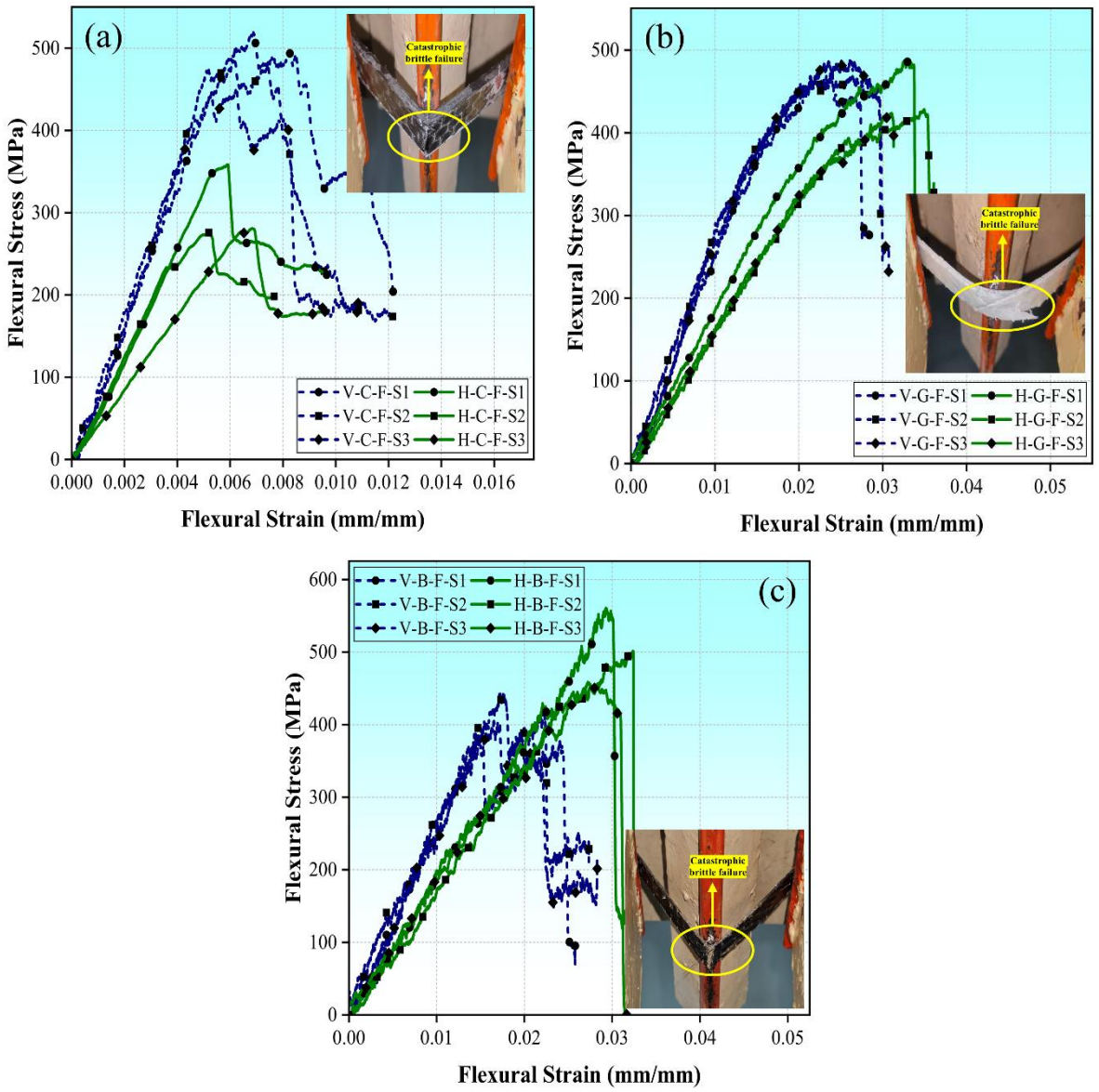


Fig. 9. Stress-strain relationship of (a) CFRP, (b) GFRP, and (c) BFRP tested under flexural loading

4.2.4. Interlaminar Shear Responses

The load-displacement responses and failure modes of the unidirectional composites evaluated under the short beam shear test are illustrated in **Fig. 10a-c**, with average interlaminar properties summarised in **Table 5**. The VARTM laminates exhibit steeper initial slopes and significantly higher peak loads within shorter displacement ranges, indicating higher interlaminar shear stiffness and load-carrying capacity. Meanwhile, the HLU laminates show

broader curves with moderate slopes, lower peak loads, and extended displacement before failure. This behavior reflects a more compliant shear response with lower peak loads and larger displacement before failure. All laminates fail through fiber-layer delamination along the neutral mid-plane, consistent with matrix-dominated interlaminar shear failure.

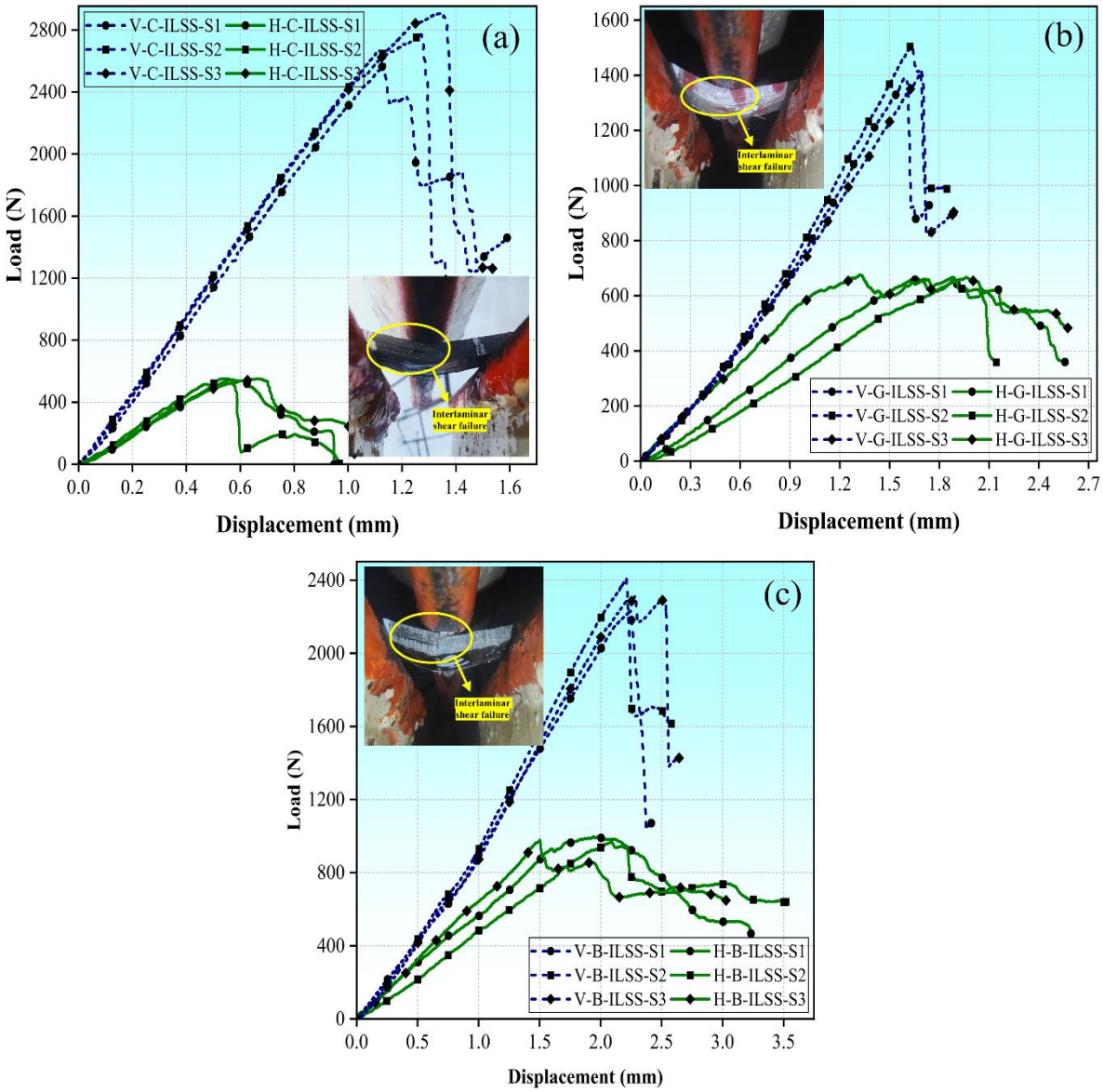


Fig. 10. Load-displacement relationship of (a) CFRP, (b) GFRP, and (c) BFRP tested under short beam test

Quantitatively, the VARTM process significantly improves interlaminar shear strength across all material categories, confirming the process-driven enhancement in the through-thickness mechanical response. The interlaminar shear strength of CFRP increases by an exceptional 320.1%, while GFRP and BFRP show increases by 103.8% and 92.1%, respectively. The massive strength deficiency observed in the HLU carbon variant demonstrates the strong sensitivity of CFRP interlaminar performance to the manufacturing route. The present findings

contradict the processing trends reported by Scalici et al. [19], where higher HLU shear strength is due to poorly impregnated zones in VARTM, but align closely with the established process-structure-property relationship observed by Varley et al. [41]. Interestingly, the VARTM process nearly doubles the interlaminar shear capacity of BFRP while reducing its flexural strength due to limitations on top-face compression. Carmisciano et al. [35] also reported a similar behavior, explaining that premature failure in BFRP occurs in the compression half-section, characterized by fiber microbuckling and kink bands. This contrasting behavior demonstrates that the influence of the manufacturing route depends strongly on the loading mode, with the flexural and interlaminar responses showing varying sensitivities.

Table 5. Average flexural and interlaminar properties of unidirectional composite laminates manufactured by HLU and VARTM

Properties	Symbol (unit)	HLU			VARTM		
		CFRP	GFRP	BFRP	CFRP	GFRP	BFRP
Flexural modulus	E_F (GPa)	55.97± (12.18%)	16.91± (2.11%)	17.88± (12.46%)	89.19± (3.96%)	28.09± (5.09%)	24.06± (2.80%)
Flexural strength	σ_F (MPa)	304.96± (15.16%)	446.05± (7.95%)	506.56± (10.13%)	486.68± (7.22%)	477.01± (2.14%)	413.58± (6.56%)
Interlaminar shear strength	τ_{ILSS} (MPa)	9.81± (0.58%)	15.35± (1.62%)	23.47± (2.47%)	41.21± (2.11%)	31.28± (4.56%)	45.10± (3.80%)

Note: values represent mean ± standard deviation (%)

4.3. Effect of processing method on the anisotropy behavior

This section briefly discusses the influence of the manufacturing process on the anisotropy behavior of unidirectional composite laminates, using stiffness and strength ratios derived from experimental results of tensile, compression, flexural, and interlaminar shear tests. The discussion highlights how manufacturing processes govern the directional stiffness and strength contrast, as well as the efficiency with which tensile-derived properties are translated into out-of-plane bending and shear responses. **Fig. 11** displays the anisotropy behavior of the composite laminates using various anisotropy indices.

4.3.1. Tensile Degrees of Anisotropy

Fig. 11a displays the tensile DA of various composite laminates. The stiffness anisotropy ratios (DA_{ET} and DA_{G12}) indicates that the influence of manufacturing methods on tensile anisotropy is strongly fiber-dependent. Both HLU and VARTM exhibit substantially higher stiffness- and

strength-based anisotropy, particularly in CFRP and GFRP laminates. The relative increase in tensile anisotropy of VARTM over HLU is more pronounced in GFRP (24.64% for DA_{ET} and 9.52% for DA_{G12}) whereas the increase is 13.21% for DA_{ET} and 0.40% for DA_{G12} in CFRP, indicating a strong sensitivity to manufacturing-induced anisotropy evolution. Conversely, under VARTM, BFRP exhibits a different anisotropy evolution, where the longitudinal tensile stiffness anisotropy decreases (17.60%) slightly, despite a simultaneous increase in the shear-stiffness ratio (15.99%). The rough surface morphology of basalt fibers may promote superior resin infiltration and inter-tow resin bridging under vacuum, resulting in a significant increase in transverse tensile stiffness relative to longitudinal stiffness. This suggests that the manufacturing process redistributes the stiffness improvements differently in BFRP compared to CFRP and GFRP, resulting in a more balanced bidirectional stiffness response while maintaining a strong directional dependence in shear.

The VARTM process also exhibits more pronounced strength-based anisotropy ($DA_{\sigma T}$) over HLU, with 42.90% for CFRP, 48.91% for GFRP, and 6.41% for BFRP, where the increase in longitudinal tensile strength exceeds the corresponding improvement in transverse strength. The failure mechanisms observed during the experiment support this trend, with VARTM exhibiting fiber-dominant failure. Conversely, the relative increase in resin content and void fraction under the HLU process allows for limited plastic deformation before failure. The relatively marginal increase in the strength anisotropy of BFRP suggests that manufacturing methods improve the longitudinal and transverse tensile strengths by almost equal amounts. Overall, the contrasting trends demonstrate that anisotropy evolution is influenced not only by absolute mechanical properties but also by the manufacturing process and fiber type.

4.3.2. Compressive Anisotropy Indices

A similar fiber-dependent anisotropy evolution is observed under compression loading **(Fig. 11b)**. VARTM exhibits higher compression anisotropy indices over HLU for CFRP (28.88% for AI_{EC} and 71.38% for $AI_{\sigma C}$) and for BFRP (111.68% for AI_{EC} and 40.28% for $AI_{\sigma C}$), indicating that the E_{C1} and X_C improves substantially more than the E_{C2} and Y_C. This behavior suggests that the VARTM process enhances the load-carrying capacity in longitudinal compression relative to transverse compression, mirroring tensile anisotropy. Interestingly, VARTM produces noticeable reductions in both AI_{EC} (67.07%) and $AI_{\sigma C}$ (81.45%) for GFRP over HLU. Despite improvements in absolute compression properties, the transition from HLU to VARTM results in a more balanced bidirectional compressive behavior. The presence of glass fiber knitting in the transverse direction contributes to the observed behavior, enhancing

the load-carrying capacity of the composite relative to CFRP and BFRP, thereby reducing anisotropy. These contrasting trends demonstrate that the same manufacturing route results in fiber-type anisotropy evolution. While VARTM displays higher directional compressive response in CFRP and BFRP, the same manufacturing method reduces anisotropy in GFRP, confirming that fiber architecture strongly influences anisotropy evolution more than enhancements in absolute compression properties.

4.3.3. Flexural and Interlaminar Shear Indices

The anisotropy indices are further extended to flexural and interlaminar shear properties to evaluate the relationship between tensile, flexural, and interlaminar shear response. Unlike the tensile and compression anisotropy indices, the flexural and interlaminar shear indices determine the translation efficiency of tensile-derived properties into corresponding flexural and interlaminar behavior. **Fig. 11c** and **d** present the flexural and interlaminar shear translational indices of the composite laminates.

The flexural stiffness anisotropy (AI_{EF}) remains close to unity for all laminates, indicating that laminates manufactured using HLU and VARTM, which exhibit relatively proportional tensile-to-bending stiffness irrespective of fiber type. The transition from HLU and VARTM shows a 17.99% reduction in AI_{EF} for CFRP, and very marginal to no measurable difference in GFRP and BFRP. Consequently, the overall tensile-to-bending stiffness translation relationship remains largely insensitive to the two manufacturing processes. In contrast, the flexural strength anisotropy ($AI_{\sigma F}$) exhibit strong dependence on fiber type and the manufacturing process. While CFRP exhibits higher anisotropy values under both manufacturing processes, with a large disparity between tensile and flexural strengths, the values are much closer to unity for GFRP and BFRP, demonstrating stronger tensile-to-bending strength translation efficiency. Collectively, the results indicate that the tensile-to-bending translational efficiency is largely preserved despite the manufacturing-induced variations, demonstrating that the relationship between tensile and flexural properties is comparatively insensitive to the manufacturing process.

The interlaminar shear anisotropy (AI_{ILSS}) reveals a different fiber-dependent response compared with the flexural translational indices. For CFRP and BFRP, VARTM significantly reduces AI_{ILSS} over HLU by 55.88% and 33.48% respectively, demonstrating that the interlaminar shear strength improves proportionately more than the longitudinal tensile strength. Conversely, GFRP exhibits a 31.64% increase in AI_{ILSS} under VARTM,

demonstrating that the improvement in longitudinal tensile strength exceeds that of the interlaminar shear strength. The presence of transverse glass fiber knitting introduces localized inter-yarn resin-rich channels that undergo shear deformation, limiting interlaminar shear stress transfer. The AI_{ILSS} exhibits greater sensitivity to both fiber type and manufacturing process than flexural indices, demonstrating the combined influence on the tensile-to-shear relationship.

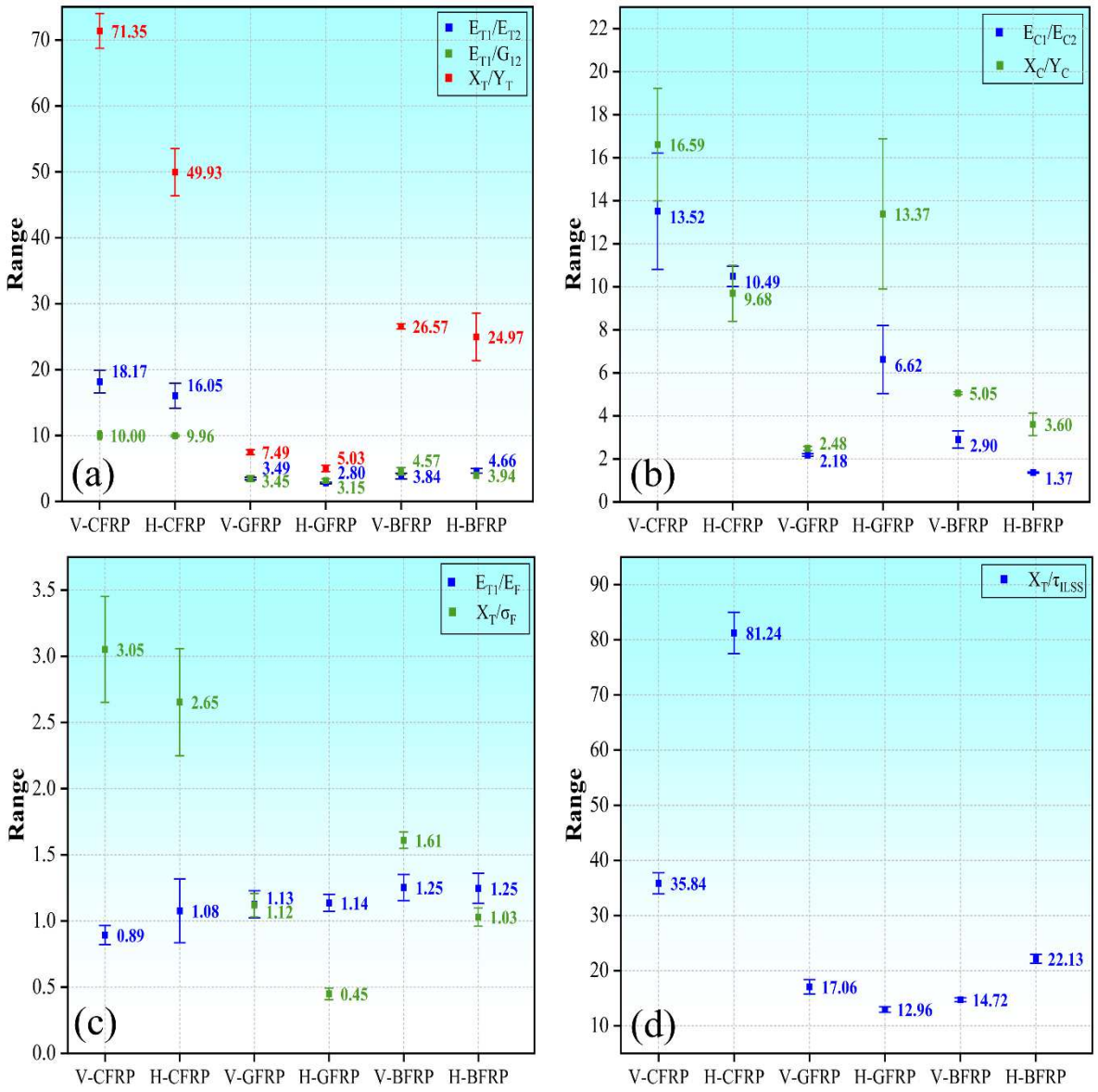


Fig. 11. Anisotropy behavior of composite laminates based on the anisotropy indices for (a) tensile, (b) compression, (c) flexural, and (d) interlaminar shear responses

The flexural and interlaminar indices demonstrate that the manufacturing process not only influences the magnitude of the mechanical properties but also the efficiency with which those properties are translated across different loading modes. While the flexural translation indices

remain relatively insensitive to the manufacturing process, the interlaminar shear translation index exhibits a combined influence of fiber type and manufacturing process. These findings underscore that the effectiveness of a manufacturing process extends beyond the conventional directional stiffness and strength and also influences the coupling between tensile, bending, and interlaminar behavior.

4.4. Statistical evaluation of mechanical properties using ANOVA

Detailed statistical calculations and verifications of ANOVA assumptions are presented in Tables S6-S9 in the supplementary file. According to the statistical analysis, fiber type (Factor B: Carbon vs E-glass vs Basalt) has a statistically significant effect on all properties, highlighting its dominant effect on the mechanical performance. The calculated F-values of fiber type are one to two orders of magnitude higher than those of the manufacturing method (Factor A: HLU vs VARTM), reinforcing the primary role of fiber selection in determining the multiaxial response. Simultaneously, the manufacturing method significantly affects nearly all properties, except for longitudinal compression strength ($p = 0.10747$). This is consistent with the experimental results (Section 4.2.2), which show that HLU CFRP and GFRP display slightly higher longitudinal compression strengths. Stiffness-related properties remain consistently sensitive to the manufacturing process, confirming that it exerts a measurable influence on the multiaxial mechanical responses across different reinforcement systems.

The two-factor interaction effects (A x B) are statistically significant for most properties, except the off-axis in-plane shear modulus ($p = 0.13094$). **Fig. 12** shows the interaction plots for tensile and in-plane shear properties. The longitudinal tensile properties exhibit substantial interaction sensitivities ($F = 25.61$ for modulus and $F = 58.34$ for strength), indicating that the improvements from VARTM are strongly fiber-dependent. As shown in **Fig. 12a** and **b**, CFRP exhibits a large increase in both longitudinal modulus and strength, whereas GFRP and BFRP configurations respond differently to the manufacturing process, resulting in the observed interaction effect. In contrast, the transverse tensile properties show lower interaction effects ($F = 14.68$ for modulus and $F = 63.37$ for strength). However, the interaction plots reveal that the manufacturing process remains reinforcement-dependent, as shown in **Fig. 12c** and **d**. BFRP shows a substantially larger improvement in transverse tensile stiffness, whereas GFRP shows more enhanced transverse tensile strength than CFRP and BFRP. The off-axis in-plane shear strength exhibited a significantly higher interaction effect ($F = 5.94$) than shear modulus ($F = 2.42$), as displayed in **Fig. 12e** and **f**, indicating that ultimate shear strength is strongly influenced by the combined process-fiber interfacial coupling rather than shear stiffness.

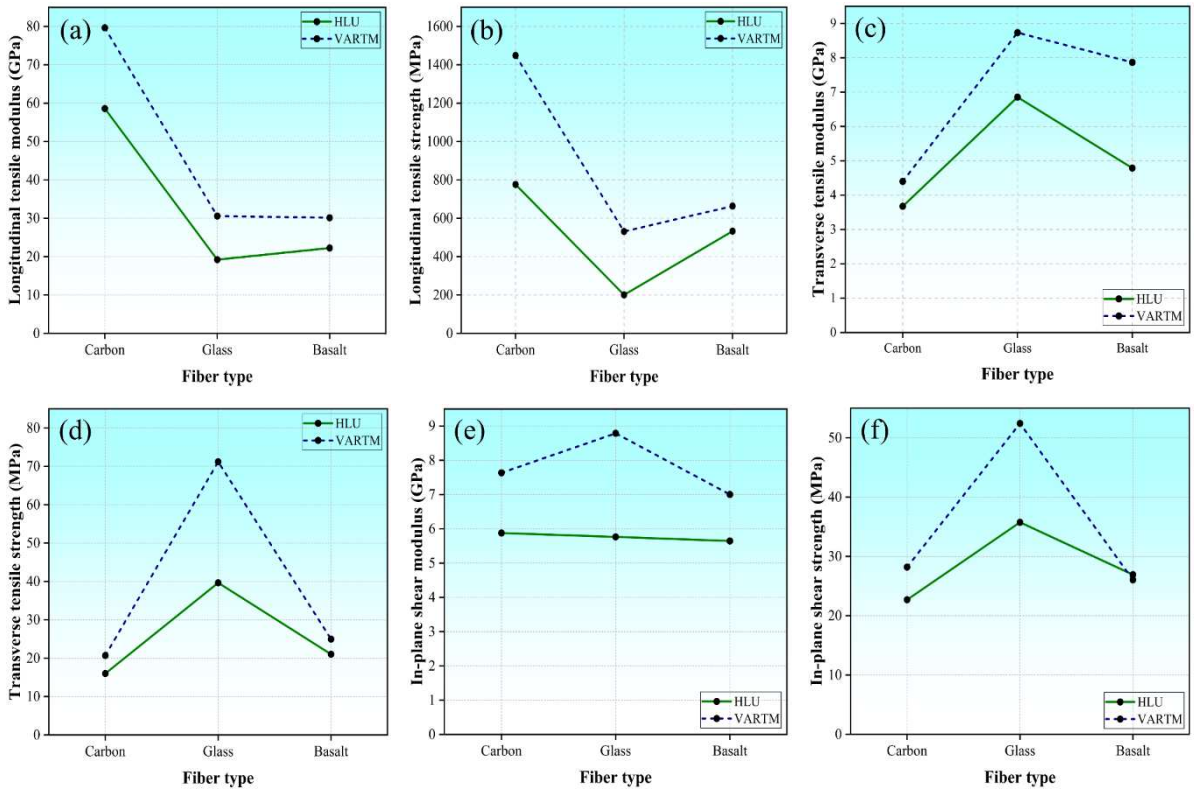


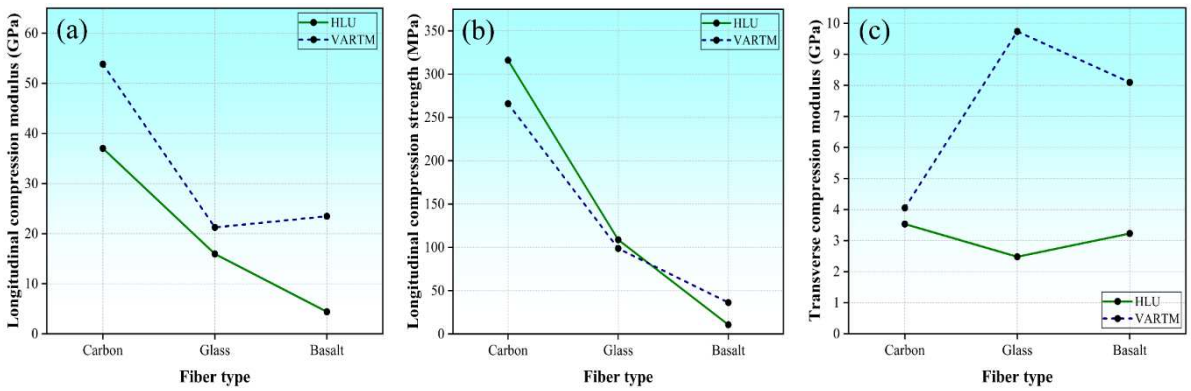
Fig. 12. Interaction plots illustrating the combined effect of manufacturing method and fiber type on (a) longitudinal tensile modulus, (b) longitudinal tensile strength, (c) transverse tensile modulus, (d) transverse tensile strength, (e) in-plane shear modulus, and (f) in-plane shear strength

Fig. 13 presents the two-way interaction plots for compression, flexural, and interlaminar shear properties. The longitudinal compression modulus and strength parameters exhibit lower interaction metrics (F = 15.18 and F = 8.49, respectively), indicating a comparatively smaller interaction effect between fiber type and manufacturing process. As observed in **Fig. 13a** and **b**, VARTM increases the longitudinal compression modulus across all reinforcement systems, whereas the influence on longitudinal compression strength varies with fiber type, resulting in higher strengths for CFRP and BFRP under HLU, but higher for VARTM BFRP. In contrast, the transverse compression properties are highly sensitive to fiber type and manufacturing process, as reflected in exceptionally high interaction values (F = 428.19 for the transverse compression modulus and F = 1429.75 for strength). This behavior is clearly visible in **Fig. 13c** and **d**, where VARTM produces dramatically different responses among the three reinforcement systems, particularly for GFRP, which exhibits a disproportionately large increase in transverse compression properties. The magnitude of these interaction effects demonstrates that transverse compression properties are considerably more sensitive to the manufacturing process than their longitudinal counterparts. These results confirm that the

response to the manufacturing process is highly dependent on the reinforcement type, especially under transverse compression loading.

The flexural modulus and strength exhibit statistically significant effects from both factors, with moderate interaction magnitudes (F = 11.01 and F = 21.02, respectively). As shown in **Fig. 13e**, VARTM increases flexural stiffness across all reinforcement systems, though the magnitude of improvement varies with fiber type and is more pronounced with CFRP. **Fig. 13f** shows a more pronounced interaction effect for flexural strength, in which the manufacturing process effect depends on fiber type. VARTM improves the flexural strength of CFRP, produces a marginal improvement in GFRP, and results in lower strength for BFRP.

In contrast, the short-beam interlaminar shear strength exhibits significant interaction effects (F = 89.97), demonstrating that interlaminar shear performance is highly fiber-dependent. As shown in **Fig. 13g**, VARTM enhances interlaminar shear strength by 320.1% for CFRP, 103.8% for GFRP, and 92.1% for BFRP, reflecting that the improvement is not consistent across all fiber systems. The HLU laminates show notably lower shear strength for CFRP and BFRP, whereas GFRP exhibits relatively minor differences across the two processing methods, indicating that the effect of manufacturing method cannot be separated from that of fiber type. The results confirm that the manufacturing process alters the interlaminar shear strength, but the magnitude of the change is fiber-dependent, demonstrating the influence of the interaction effect on the interlaminar shear response.



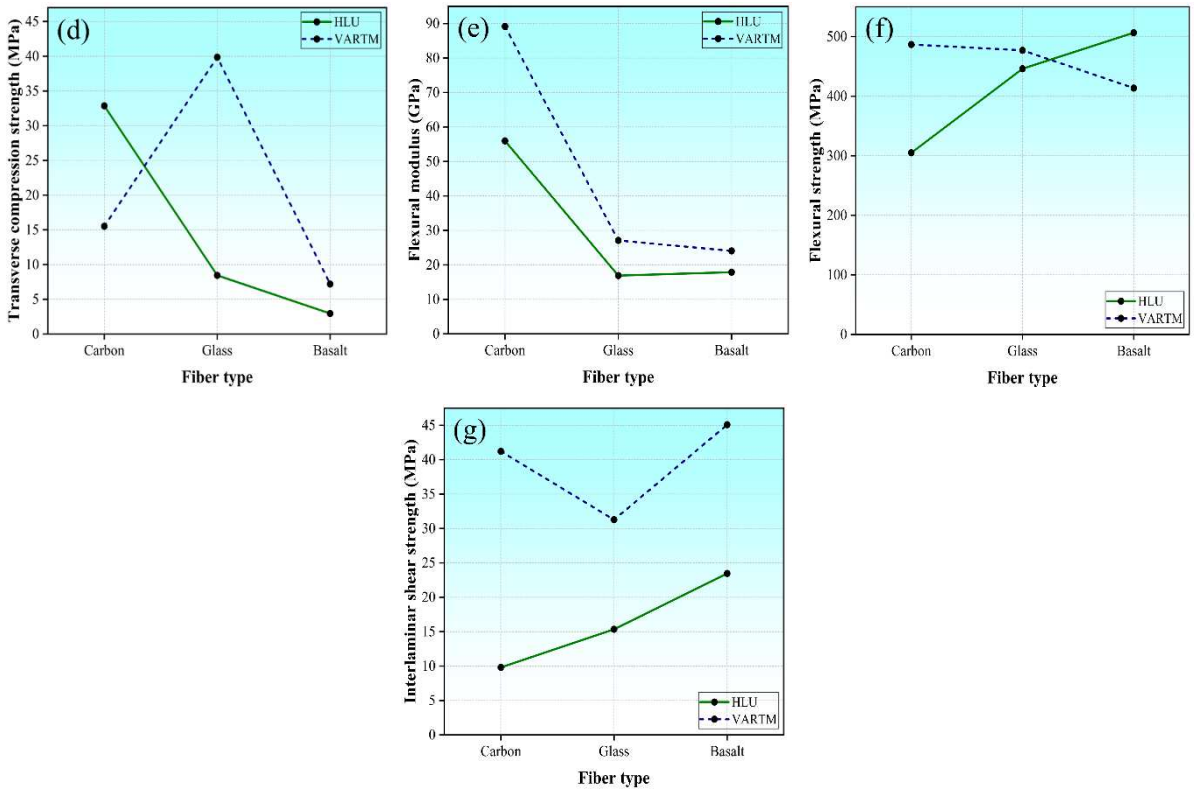


Fig. 13. Interaction plots illustrating the combined effect of manufacturing method and fiber type on (a) longitudinal compression modulus, (b) longitudinal compression strength, (c) transverse compression modulus, (d) transverse compression strength, (e) flexural modulus, (f) flexural strength, and (g) interlaminar shear strength

Overall, the two-way ANOVA results confirm that fiber selection predominantly governs longitudinal stiffness and strength, as well as in-plane responses. Conversely, matrix- and interface-dominant properties, specifically transverse compression and interlaminar shear, are highly sensitive to the combined interaction effect of fiber type and manufacturing process. These statistical evaluations are consistent with the experimentally observed process-structure-mechanics relationships. While fiber selection primarily controls the overall magnitude of mechanical properties, the influence of the manufacturing process varies significantly across different reinforcement systems and loading modes, particularly for transverse compression and interlaminar shear responses.

4.5. Impact on Automotive Applications

The results presented in this study provide useful insights for the selection and processing of lightweight automotive composite structures. Among the investigated laminates, VARTM-processed CFRP exhibits the highest longitudinal tensile, flexural, and interlaminar shear performance, which makes it suitable for stiffness-critical and load-bearing components.

However, the high anisotropy observed in CFRP indicates the importance of considering directional mechanical behavior during laminate design and structural optimization. GFRP exhibits relatively lower longitudinal stiffness than CFRP but demonstrates comparatively improved transverse and flexural behavior, especially under VARTM. This behavior indicates a more balanced directional mechanical behavior, which suggests its suitability for cost-effective automotive structures subjected to multiaxial loading conditions. BFRP exhibits competitive flexural and interlaminar shear performance and greater sustainability potential than CFRP, making it attractive for automotive components, offering a favorable balance between stiffness and mechanical performance.

The comparison of HLU and VARTM further demonstrates that the manufacturing process plays a vital role in determining the final mechanical performance of the composite laminates. The density, fiber volume fraction, void content, and mechanical properties results consistently show that VARTM produces more efficient composite laminates with superior stiffness, strength, and interlaminar performance. These findings indicate that selecting the manufacturing process is also vital, alongside fiber selection, for the design of composite-based structures for automotive applications.

5. Conclusions

This study systematically investigated the effects of the manufacturing process on the multiaxial mechanical behavior and the evolution of anisotropy in unidirectional CFRP, GFRP, and BFRP composite laminates manufactured using HLU and VARTM. The results demonstrate that the manufacturing process shows distinct density, fiber volume fraction, and void fraction, which significantly influence the stiffness, strength, and anisotropic mechanical responses of the laminates.

Across all fibers, VARTM produces higher density, fiber volume fraction, and lower void content, resulting in enhanced stiffness-dominated responses, efficient load transfer, and improved overall mechanical performance. Despite its lower fiber volume fraction and higher void content, HLU exhibits comparatively higher longitudinal compression strength for CFRP and GFRP. These microstructural variations result in apparent shifts in anisotropy, with VARTM exhibiting higher tensile and compressive anisotropies in both CFRP and BFRP, highlighting fiber-dominant load transfer. However, the knitted architecture and enhanced transverse load of GFRP under VARTM reduce the compression and flexural anisotropy. For CFRP and BFRP, flexural anisotropy indices remain largely unaffected by the manufacturing

process, indicating the stable stiffness transfer from uniaxial tensile to bending. Interlaminar shear indices confirm that VARTM improves shear transfer efficiency and delamination resistance in CFRP and BFRP, while the transverse knitting may limit shear efficiency in GFRP.

Two-way ANOVA further demonstrates that fiber type has a dominant influence on all constitutive behavior, while the manufacturing process significantly affects nearly all parameters, except for longitudinal compression strength. Interaction effects are also significant, except for the in-plane shear modulus. Fiber-dominated longitudinal responses exhibit comparatively lower interaction effects, indicating lower sensitivity to the combined influence of fiber type and manufacturing process. Conversely, matrix-dominant properties, such as transverse compression and interlaminar shear strength, exhibit statistically strong sensitivity to process-fiber coupling.

Overall, the results demonstrate that the fiber type governs the fundamental mechanical response of the laminate. In contrast, the magnitude and directional balance of the resulting properties are significantly influenced by the manufacturing process. The anisotropies and translation indices developed in this study provide an additional framework for evaluating the effect of manufacturing process on the mechanical response of composite laminates under different loading modes, thereby supporting the design and optimization of lightweight automotive composite structures.

Funding Details

The research work is financially supported by the Aeronautics Research and Development Board, Defense Research and Development Organization (DRDO), New Delhi, India, [Scheme No: ARDB/01/1082030/M/I].

Data Availability Statement

The experimental data are available upon request.

Clinical Trial Registration

Not applicable.

Ethics, Consent to Participate, and Consent to Publish Declarations

Not applicable.

6. References

[1] A. Mayyas, M. Omar, M. Hayajneh, and A. R. Mayyas, "Vehicle's Lightweight Design vs. Electrification from Life Cycle Assessment Perspective," *J. Clean. Prod.*, vol. 167, pp. 687–701, 2017, doi: 10.1016/j.jclepro.2017.08.145.

[2] J. Holbery and D. Houston, "Natural-Fiber-Reinforced Polymer Composites in Automotive Applications," *JOM*, vol. 58, pp. 80–86, 2006, doi: 10.1007/s11837-006-0234-2.

[3] B. Du, Q. Li, C. Zheng, S. Wang, C. Gao, and L. Chen, "Application of Lightweight Structure in Automobile Bumper Beam: A Review," *Materials*, vol. 16, no. 3, p. 967, 2023, doi: 10.3390/ma16030967.

[4] P. Feraboli and A. Masini, "Development of Carbon/Epoxy Structural Components for a High Performance Vehicle," *Compos. B Eng.*, vol. 35, no. 4, pp. 323–330, 2004, doi: 10.1016/j.compositesb.2003.11.010.

[5] I. S. Abbood, S. A. Odaa, K. F. Hasan, and M. A. Jasim, "Properties Evaluation of Fiber Reinforced Polymers and their Constituent Materials used in Structures – A Review," *Mater. Today Proc.*, vol. 43, pp. 1003–1008, 2021, doi: 10.1016/J.MATPR.2020.07.636.

[6] B. D. Agarwal, L. J. Broutman, and K. Chandrashekhara, *Analysis and Performance of Fiber Composites*, 4th ed. Wiley, 2017. [Online]. Available: www.wiley.com/go/permissions.

[7] S. Mazumdar, *Composites Manufacturing: Materials, Product, and Process Engineering*, 1st ed. CRC Press, 2001. doi: 10.1201/9781420041989.

[8] D. K. Rajak, P. H. Wagh, and E. Linul, "Manufacturing Technologies of Carbon/Glass Fiber-Reinforced Polymer Composites and their Properties: A Review," *Polymers (Basel).*, vol. 13, no. 21, p. 3721, 2021, doi: 10.3390/polym13213721.

[9] J. Shi *et al.*, "Bamboo Fiber-Reinforced Epoxy Composites Fabricated by Vacuum-Assisted Resin Transfer Molding (VARTM): Effect of Molding Sequence and Fiber Content," *Polym. Compos.*, vol. 45, no. 1, pp. 256–266, 2023, doi: 10.1002/pc.27774.

[10] Y.-H. Kim, J.-H. Son, B.-K. Choi, Y.-D. Jo, K.-J. Kim, and J.-W. Han, "Evaluation of Mechanical Properties of CFRP by VARTM and its Applications," *Int. J. Mod. Phys. B*, vol. 20, no. 25n27, pp. 3896–3901, 2006, doi: 10.1142/S0217979206040556.

[11] S. Rohman *et al.*, "The Effect of Manufacture Process on Mechanical Properties of Epoxy-Based Carbon Fiber Composites," *AIP Conf. Proc.*, vol. 3003, no. 1, p. 020080, 2024, doi: 10.1063/5.0186304.

[12] Ç. Uzay, A. Çetin, and N. Geren, "Physical and Mechanical Properties of Laminar Composites depending on the Production Methods: An Experimental Investigation," *Sādhanā*, vol. 47, no. 4, p. 262, 2022, doi: 10.1007/s12046-022-01995-z.

[13] M. Choudhary, A. Sharma, M. Dwivedi, and A. Patnaik, "A Comparative Study of the Physical, Mechanical and Thermo-Mechanical Behavior of GFRP Composite based on Fabrication Techniques," *Fibers and Polymers*, vol. 20, no. 4, pp. 823–831, 2019, doi: 10.1007/s12221-019-8863-6.

[14] K. Abdurohman *et al.*, "A Comparison Process between Hand Layup, Vacuum Infusion and vacuum Bagging Method toward E-Glass EW 185/Lycal Composites," *Indonesian Journal of Aerospace*, vol. 21, no. 1, pp. 39–50, 2023, doi: 10.59981/ijoa.2023.286.

[15] K. C. Nagaraja, A. Manjunath, K. G. Pranesh, G. Rajeshkumar, M. G. Raju, and S. G. Shastry, "Impact of Manufacturing Methods on the Mechanical Characteristics of Polymer Matrix Composites with Glass and Epoxy Fiber Reinforcement," *Journal of The Institution of Engineers (India): Series D*, 2024, doi: 10.1007/s40033-024-00818-1.

[16] G. Batha, S. K. Mahapatra, and A. Satapathy, "A Comparison of Fabrication Routes and Property Evaluation Methods for Bio-Particulate Filled Glass-Epoxy Composites," *Polym. Compos.*, vol. 45, no. 15, pp. 14302–14317, 2024, doi: 10.1002/pc.28771.

[17] S. Selcuk, U. Ahmetoglu, and E. C. Gokce, "Basalt Fiber Reinforced Polymer Composites (BFRP) other than Rebars: A Review," *Mater. Today Commun.*, vol. 37, p. 107359, Dec. 2023, doi: 10.1016/J.MTCOMM.2023.107359.

[18] M. Sato, Y. Kataoka, M. Higashide, Y. Ishida, and S. Sugimoto, "Evaluation of the Mechanical Properties of Highly Oriented Recycled Carbon Fiber Composites using the Vacuum-Assisted Resin Transfer Molding, Wet-Layup, and Resin Transfer Molding Methods," *Polymers (Basel).*, vol. 17, no. 10, p. 1293, 2025, doi: 10.3390/polym17101293.

[19] T. Scalici, G. Pitarresi, D. Badagliacco, V. Fiore, and A. Valenza, "Mechanical Properties of Basalt Fiber Reinforced Composites Manufactured with Different Vacuum Assisted

Impregnation Techniques," *Compos. B Eng.*, vol. 104, pp. 35–43, 2016, doi: 10.1016/J.COMPOSITESB.2016.08.021.

[20] O. A. Khondker, T. Fukui, M. Inoda, A. Nakai, and H. Hamada, "Fabrication and Mechanical Properties of Aramid/Nylon Plain Knitted Composites," *Compos. Part A Appl. Sci. Manuf.*, vol. 35, no. 10, pp. 1195–1205, Oct. 2004, doi: 10.1016/J.COMPOSITESA.2004.03.004.

[21] M. Marvi-Mashhadi, C. S. Lopes, and J. LLorca, "Effect of Anisotropy on the Mechanical Properties of Polyurethane Foams: An Experimental and Numerical Study," *Mechanics of Materials*, vol. 124, pp. 143–154, Sep. 2018, doi: 10.1016/J.MECHMAT.2018.06.006.

[22] S. Hamanaka, C. Nonomura, T. B. N. Thi, and A. Yokoyama, "Correlation between Fiber Orientation Distribution and Mechanical Anisotropy in Glass-Fiber-Reinforced Composite Materials," *Journal of Polymer Engineering*, vol. 39, no. 7, pp. 653–660, 2019, doi: 10.1515/polyeng-2018-0371.

[23] E. Kessler, R. Gadow, and J. Straub, "Basalt, Glass and Carbon Fibers and their Fiber Reinforced Polymer Composites under Thermal and Mechanical Load," *AIMS Mater. Sci.*, vol. 3, no. 4, pp. 1561–1576, 2016, doi: 10.3934/matersci.2016.4.1561.

[24] W. Wang, Y. Zhang, Z. Mo, N. Chouw, K. Jayaraman, and Z. Dong Xu, "A Critical Review on the Properties of Natural Fiber Reinforced Concrete Composites Subjected to Impact Loading," *Journal of Building Engineering*, vol. 77, 2023, doi: 10.1016/j.jobe.2023.107497.

[25] ASTM International, "ASTM Designation D792-20: Standard Test Methods for Density and Specific Gravity (Relative Density) of Plastics by Displacement," in *ASTM Volume 08.01: Plastics (I): C1147– D3159*, vol. 08.01, West Conshohocken, PA, 2020. doi: 10.1520/D0792-20.

[26] ASTM International, "ASTM Designation D3171−15: Standard Test Methods for Constituent Content of Composite Materials," in *ASTM Volume 15.03: Space Simulation; Aerospace and Aircraft; Composite Materials*, vol. 15.03, West Conshohocken, PA, 2015. doi: 10.1520/D3171-15.

[27] ASTM International, “ASTM Designation D3039/D3039M−17: Standard Test Method for Tensile Properties of Polymer Matrix Composite Materials,” in *ASTM Volume 15.03: Space Simulation; Aerospace and Aircraft; Composite Materials*, vol. 15.03, West Conshohocken, PA, 2017. doi: 10.1520/D3039_D3039M-17.

[28] ASTM International, “ASTM Designation D3518/D3518M-18: Standard Test Method for In-Plane Shear Response of Polymer Matrix Composite Materials by Tensile Test of a ±45° Laminate,” in *ASTM Volume 15.03: Space Simulation; Aerospace and Aircraft; Composite Materials*, vol. 15.03, West Conshohocken, PA, 2018. doi: 10.1520/D3518_D3518M-18.

[29] ASTM International, “ASTM Designation D3410/D3410M−16: Standard Test Method for Compressive Properties of Polymer Matrix Composite Materials with Unsupported Gage Section by Shear Loading,” in *ASTM Volume 15.03: Space Simulation; Aerospace and Aircraft; Composite Materials*, vol. 15.03, West Conshohocken, PA, 2016. doi: 10.1520/D3410_D3410M-16E01.

[30] ASTM International, “ASTM Designation D6641/D6641M−16e2: Standard Test Method for Compressive Properties of Polymer Matrix Composite Materials using a Combined Loading Compression (CLC) Test Fixture,” in *ASTM Volume 15.03: Space Simulation; Aerospace and Aircraft; Composite Materials*, vol. 15.03, West Conshohocken, PA: ASTM International, 2023. doi: 10.1520/D6641_D6641M-16E02.

[31] ASTM International, “ASTM Designation D7264/D7264M-07: Standard Test Method for Flexural Properties of Polymer Matrix Composite Materials,” in *ASTM Volume 15.03: Space Simulation; Aerospace and Aircraft; Composite Materials*, vol. 15.03, West Conshohocken, PA, 2007. doi: 10.1520/D7264_D7264M-07.

[32] ASTM International, “ASTM Designation D2344/D2344M-22: Standard Test Method for Short-Beam Strength of Polymer Matrix Composite Materials and their Laminates,” in *ASTM Volume 15.03: Space Simulation; Aerospace and Aircraft; Composite Materials*, vol. 15.03, West Conshohocken, PA, 2022. doi: 10.1520/D2344_D2344M-22.

[33] I. M. Daniel and Ori. Ishai, *Engineering Mechanics of Composite Materials*, 2nd ed. Oxford University Press, 2005.

[34] A. Dorigato and A. Pegoretti, “Flexural and Impact Behavior of Carbon/Basalt Fibers Hybrid Laminates,” *J. Compos. Mater.*, vol. 48, no. 9, pp. 1121–1130, 2014, doi: 10.1177/0021998313482158.

[35] S. Carmisciano, I. M. De Rosa, F. Sarasini, A. Tamburrano, and M. Valente, “Basalt Woven Fiber Reinforced Vinylester Composites: Flexural and Electrical Properties,” *Mater. Des.*, vol. 32, no. 1, pp. 337–342, Jan. 2011, doi: 10.1016/J.MATDES.2010.06.042.

[36] A. R. Chambers, J. S. Earl, C. A. Squires, and M. A. Suhot, “The Effect of Voids on the Flexural Fatigue Performance of Unidirectional Carbon Fiber Composites Developed for Wind Turbine Applications,” *Int. J. Fatigue*, vol. 28, no. 10, pp. 1389–1398, Oct. 2006, doi: 10.1016/J.IJFATIGUE.2006.02.033.

[37] S. A. Elnekhaily and R. Talreja, “Effects of Micro Voids on the Early Stage of Transverse Crack Formation in Unidirectional Composites,” *Compos. Part A Appl. Sci. Manuf.*, vol. 167, p. 107457, 2023, doi: 10.1016/J.COMPOSITESA.2023.107457.

[38] B. D. Harper, G. H. Staab, and R. S. Chen, “A Note on the Effects of Voids upon the Hygral and Mechanical Properties of AS4/3502 Graphite/Epoxy,” *J. Compos. Mater.*, vol. 21, no. 3, pp. 280–289, 1987, doi: 10.1177/002199838702100306.

[39] N. Kuentzer, P. Simacek, S. G. Advani, and S. Walsh, “Correlation of Void Distribution to VARTM Manufacturing Techniques,” *Compos. Part A Appl. Sci. Manuf.*, vol. 38, no. 3, pp. 802–813, 2007, doi: 10.1016/J.COMPOSITESA.2006.08.005.

[40] W. Sun, Z. Guan, Z. Li, M. Zhang, and Y. Huang, “Compressive Failure Analysis of Unidirectional Carbon/Epoxy Composite based on Micro-Mechanical Models,” *Chinese Journal of Aeronautics*, vol. 30, no. 6, pp. 1907–1918, 2017, doi: 10.1016/J.CJA.2017.10.002.

[41] R. J. Varley, W. Tian, K. H. Leong, A. Y. Leong, F. Fredo, and M. Quaresimin, “The Effect of Surface Treatments on the Mechanical Properties of Basalt-Reinforced Epoxy Composites,” *Polym. Compos.*, vol. 34, no. 3, pp. 320–329, 2013, doi: 10.1002/pc.22412.

Supplementary Files

This is a list of supplementary files associated with this preprint. Click to download.

- Supplementarydata.docx